March 26, 2026

Jeonghoon Lee, Ph. D

Professor
Dept. of Science Education
Ewha Womans University
Seoul 120-750, Korea
Email: jeonghoon.d.lee@gmail.com
Tel: +82-2-3277-3794

Dear Editor Gabriele Messori,

We are pleased to resubmit the revised version of our manuscript entitled *"Climate-related signals in the GV7-C ice core from East Antarctica for 1782–2013 CE: Potential relevance to climate and teleconnections between tropics and Antarctica"* for consideration in Earth System Dynamics.

We sincerely appreciate all the comments and suggestions provided. We have carefully addressed all comments and detailed responses are provided below.

Note to editor: Compared to the previous revision (submitted on 24 Feb 2026), we have edited/described the method section more clearly (highlighted in red text below) and correlation analysis.

2.3 Climate data and analysis

The $\delta^{18}O$ ($\delta^{18}O$ is preferred because it is highly correlated with δD; r = 0.99), *d*-excess, and SA from the GV7-C ice core were used in the correlation analysis. Two time periods (1957–2013 CE and 1872–2013 CE) were selected for correlation analyses between GV7-C records and climate variables based on data availability (e.g., SAM indices) and to ensure adequate sample size. The annual means of the ice core records derived from multiple intra-annual samples (3–21 data points per year; average 8) were used in the correlation analysis, which reduces the influence of seasonal extreme values. Because isotopic composition recorded in an annual layer reflects integrated snowfall through the year, GV7-C records represent the combined influence of seasonal processes. For the climate data, we therefore examined at both annual (January–December) and seasonal (DJF, MAM, JJA, SON) scales to assess potential relationships. Although some seasonal differences were observed, overall patterns and physical interpretations were consistent when annual means were used; therefore, annual values are presented to represent the net integrated climate signal preserved in the ice core. Correlation analyses were conducted on original and linearly detrended time series (annual and three-year running averages) of the ice core and climate data, and the results are described in Sections 3.3.1 – 3.3.2. The correlation analysis on the smoothed time series were conducted to reduce stratigraphic noise, and at least three-year averaging has been suggested for obtaining a significant climatic signal from the GV7 site (e.g., Frezzotti et al., 2007; Khan et al., 2021; Schlosser and Oerter, 2002). Pearson correlation coefficients were calculated and their significance was assessed using a two-tailed Student's t-test with corresponding *p*-values. Although, the ice core and climate data were annually averaged and linear trends were removed, the effects of autocorrelation on the correlation analysis were also tested using effective number of degrees of freedom (N_{eff}) (at $p < 0.05$) (Bretherton et al., 1999). The results indicated negligible autocorrelation effects on the reported correlations (for the correlation coefficients in Tables 4 and 6), and thus the correlations can be considered statistically robust.

For the 1957–2013 CE period, the following climate indices were compared with the annual means of the GV7-C ice core

We improved the description about data distribution and linearization, detrending. The analyses are conducted on annual means of the ice core and climate data. Annual averaging reduces the influence of seasonal extreme values. For the ice core records, depending on the resolution of the records (3–21 data points per year), we were not able obtain continuous seasonal values. For the climate data, we tested/examined at both annual and seasonal (DJF, MAM, JJA, SON) scales to assess potential relationships. Overall patterns and physical interpretations were consistent when annual means were used; therefore, annual values of the climate data were used in the correlation analysis.

We have also considered detrending on the time series, in the correlation analyses, we conducted on the original and linearly detrended (removed linear trends to compare the fluctuations in the ice core and climate data) time series of the ice core and climate data, and the results are described in Sections 3.3.1 – 3.3.2. We have also conducted the correlation analysis on annual and three-year running averages. The correlation analysis on the smoothed time series (three-year running averages) were conducted to reduce stratigraphic noise, and at least three-year averaging also has been suggested for obtaining a significant climatic signal from the GV7 site (e.g., Frezzotti et al., 2007; Khan et al., 2021; Schlosser and Oerter, 2002). Pearson correlation coefficients were calculated and their significance was assessed using a two-tailed Student's t-test with corresponding *p*-values.

We also considered the effect of autocorrelation, although, the ice core and climate data were already annually averaged and linear trends were removed. The effects of autocorrelation on the correlation analysis were tested using effective number of degrees of freedom (N_{eff}) at $p < 0.05$ (Bretherton et al., 1999). The results indicated negligible autocorrelation effects on the reported correlations in Tables 4 and 6 (highlighted blue in below tables), and thus the correlations can be considered statistically robust. We mentioned the autocorrelation effects in the materials and method section of the revised manuscript.

Table 4. Pearson's correlation coefficients (r) between the GV7-C ice core records and the climate variables for the period 1957–2013 CE. Correlations are calculated for annual data and three-year running averages in the detrended and original time series (shown in parentheses). Larger values ($r > 0.3$ at $p < 0.05$) are marked in bold. SIE (EA) and SIE (RA) denotes sea ice extent over East Antarctica and the Ross-Amundsen Sea sector.

	IOD	SST (SEIO)	SAM	SOI	Niño3.4	SIE (EA)	SIE (RA)
Annual average							
SA	**0.37** (0.28) Neff ≈ N, indicating negligible autocorrelation effects, at p < 0.001	–0.22 (–0.26)	0.12 (0.04)	–0.00 (–0.01)	0.04 (0.04)	0.01 (–0.02)	0.09 (0.00)
$\delta^{18}O$	–0.01 (–0.03)	–0.06 (–0.07)	–0.18 (–0.18)	–0.26 (-0.26)	0.22 (0.22)	–0.06 (–0.07)	–0.23 (–0.22)
d-excess	–0.19 (–0.07)	0.25 **(0.33)**	–0.03 (0.09)	0.02 (0.03)	0.04 (0.05)	–0.05 (0.02)	0.11 (0.22)
Three-year running average							
SA	**0.39** (0.18) Neff ≈ N, indicating negligible autocorrelation effects, at p < 0.0001	**–0.30 (–0.36)** Neff ≈ N, indicating negligible autocorrelation effects, at p < 0.05	0.11 (–0.06)	0.09 (0.09)	–0.11 (–0.14)	0.11 (0.04)	–0.18 (–0.02)

			–0.41 (–0.27)	**–0.49 (–0.49)**	**0.46 (0.46)**		**–0.47 (–0.32)**
$\delta^{18}O$	–0.06 (–0.02)	0.02 (0.04)	Neff ≈ N, indicating negligible autocorrelation effects, at p < 0.0017	Neff ≈ N, indicating negligible autocorrelation effects, at p < 0.0001	Neff ≈ N, indicating negligible autocorrelation effects, at p < 0.0004	–0.14 (–0.11)	Neff ≈ N, indicating negligible autocorrelation effects, at p < 0.0002
	–0.45 (–0.06)	**0.64 (0.72)**				**–0.35** (–0.16)	
d-excess	Neff ≈ N, indicating negligible autocorrelation effects, at p < 0.0005	Neff ≈ N, indicating negligible autocorrelation effects, at p < 0.0001	–0.15 (–0.21)	–0.11 (–0.09)	0.24 (0.27)	Neff ≈ N, indicating negligible autocorrelation effects, at p < 0.0092	0.01 (0.31)

Table 6. Pearson's correlation coefficients (r) between the GV7-C ice core records and the climate variables for the period 1872–2013 CE. Correlations are calculated for annual data and three-year running averages in the detrended and original time series (shown in parentheses). Larger values (r > 0.3 at $p < 0.05$) are marked in underlined bold.

	IOD	SST (SEIO)	SST anomaly	SAM	Niño3.4
Annual average					
SA	0.10 (0.10)	–0.15 (–0.11)	–0.03 (–0.01)	0.03 (0.03)	0.02 (0.02)
$\delta^{18}O$	–0.04 (–0.04)	–0.01 (–0.02)	–0.10 (–0.08)	–0.16 (–0.14)	0.14 (0.13)
d-excess	–0.02 (0.08)	0.02 (0.28)	–0.20 (0.28)	0.06 (0.18)	0.12 (0.13)
Three-year running average					
SA	–0.04 (0.01)	–0.02 (0.02)	–0.04 (0.02)	0.00 (0.04)	0.02 (0.03)
$\delta^{18}O$	–0.12 (–0.11)	0.00 (–0.02)	–0.13 (–0.11)	–0.23 (–0.16)	0.19 (0.18)
	0.03 (0.23)	**0.32 (0.43)**	0.26 **(0.39)**	–0.02 (0.24)	0.24 (0.26)
d-excess		Neff ≈ N, indicating negligible autocorrelation effects, at p < 0.00017			

We have excluded the correlation results on 5-year running averaged as well as 3- and 5-year (point) averages in the revised version, which we considered as unnecessary details. We have revised Section 2.3 as shown below.

Accordingly, we edited the correlation analysis (Tables 4, 6 and Figures 3, 4)

Table 4. Pearson's correlation coefficients (r) between the GV7-C ice core records and the climate variables for the period 1957–2013 CE. Correlations are calculated for annual data and three-year running averages in the detrended and original time series (shown in parentheses). Larger values (r > 0.3 at $p < 0.05$) are marked in bold. SIE (EA) and SIE (RA) denotes sea ice extent over East Antarctica and the Ross-Amundsen Sea sector.

	IOD	SST (SEIO)	SAM	SOI	Niño3.4	SIE (EA)	SIE (RA)
Annual average							

SA	**0.37** (0.28)	–0.22 (–0.26)	0.12 (0.04)	–0.00 (–0.01)	0.04 (0.04)	0.01 (–0.02)	0.09 (0.00)
$\delta^{18}O$	–0.01 (–0.03)	–0.06 (–0.07)	–0.18 (–0.18)	–0.26 (-0.26)	0.22 (0.22)	–0.06 (–0.07)	–0.23 (–0.22)
d-excess	–0.19 (–0.07)	0.25 **(0.33)**	–0.03 (0.09)	0.02 (0.03)	0.04 (0.05)	–0.05 (0.02)	0.11 (0.22)
Three-year running average							
SA	**0.39** (0.18)	**–0.30 (–0.36)**	0.11 (–0.06)	0.09 (0.09)	–0.11 (–0.14)	0.11 (0.04)	–0.18 (–0.02)
$\delta^{18}O$	–0.06 (–0.02)	0.02 (0.04)	**–0.41** (–0.27)	**–0.49 (–0.49)**	**0.46 (0.46)**	–0.14 (–0.11)	**–0.47 (–0.32)**
d-excess	**–0.45** (–0.06)	**0.64 (0.72)**	–0.15 (–0.21)	–0.11 (–0.09)	0.24 (0.27)	**–0.35** (–0.16)	0.01 (0.31)

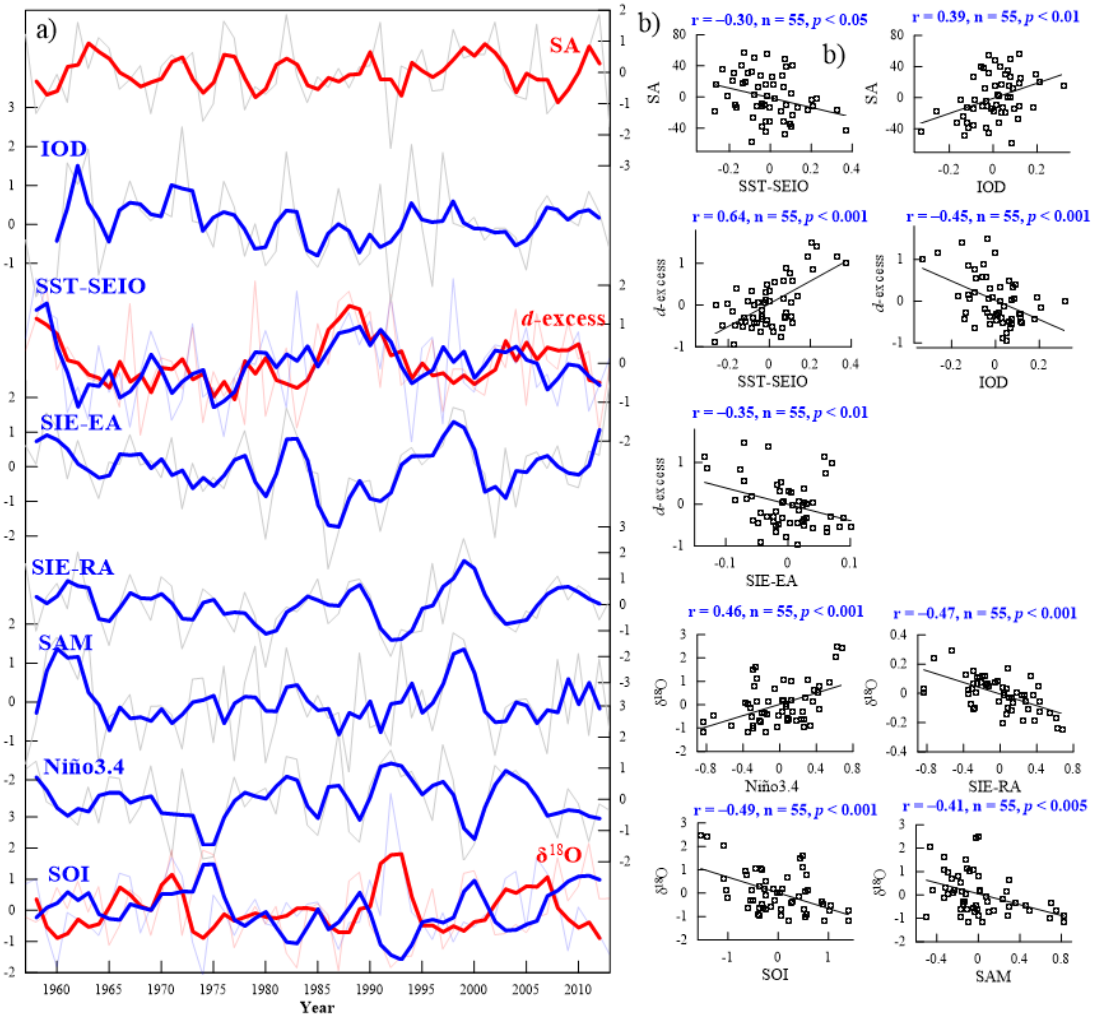


Figure 3. Comparison of the standardized profiles (grey lines) for detrended time series of SA, $\delta^{18}O$, and *d*-excess with the climate variables for 1957–2013 CE (a). The thick lines (blue and red) indicate

the 3-year running average. Linear regression profiles for the 3-year running averaged time series are also shown with significant correlation coefficients (at $p < 0.05$) (b).

Table 6. Pearson's correlation coefficients (r) between the GV7-C ice core records and the climate variables for the period 1872–2013 CE. Correlations are calculated for annual data and three-year running averages in the detrended and original time series (shown in parentheses). Larger values ($r > 0.3$ at $p < 0.05$) are marked in underlined bold.

	IOD	SST (SEIO)	SST anomaly	SAM	Niño3.4
Annual average					
SA	0.10 (0.10)	–0.15 (–0.11)	–0.03 (–0.01)	0.03 (0.03)	0.02 (0.02)
$\delta^{18}O$	–0.04 (–0.04)	–0.01 (–0.02)	–0.10 (–0.08)	–0.16 (–0.14)	0.14 (0.13)
d-excess	–0.02 (0.08)	0.02 (0.28)	–0.20 (0.28)	0.06 (0.18)	0.12 (0.13)
Three-year running average					
SA	–0.04 (0.01)	–0.02 (0.02)	–0.04 (0.02)	0.00 (0.04)	0.02 (0.03)
$\delta^{18}O$	–0.12 (–0.11)	0.00 (–0.02)	–0.13 (–0.11)	–0.23 (–0.16)	0.19 (0.18)
d-excess	0.03 (0.23)	**0.32 (0.43)**	0.26 **(0.39)**	–0.02 (0.24)	0.24 (0.26)

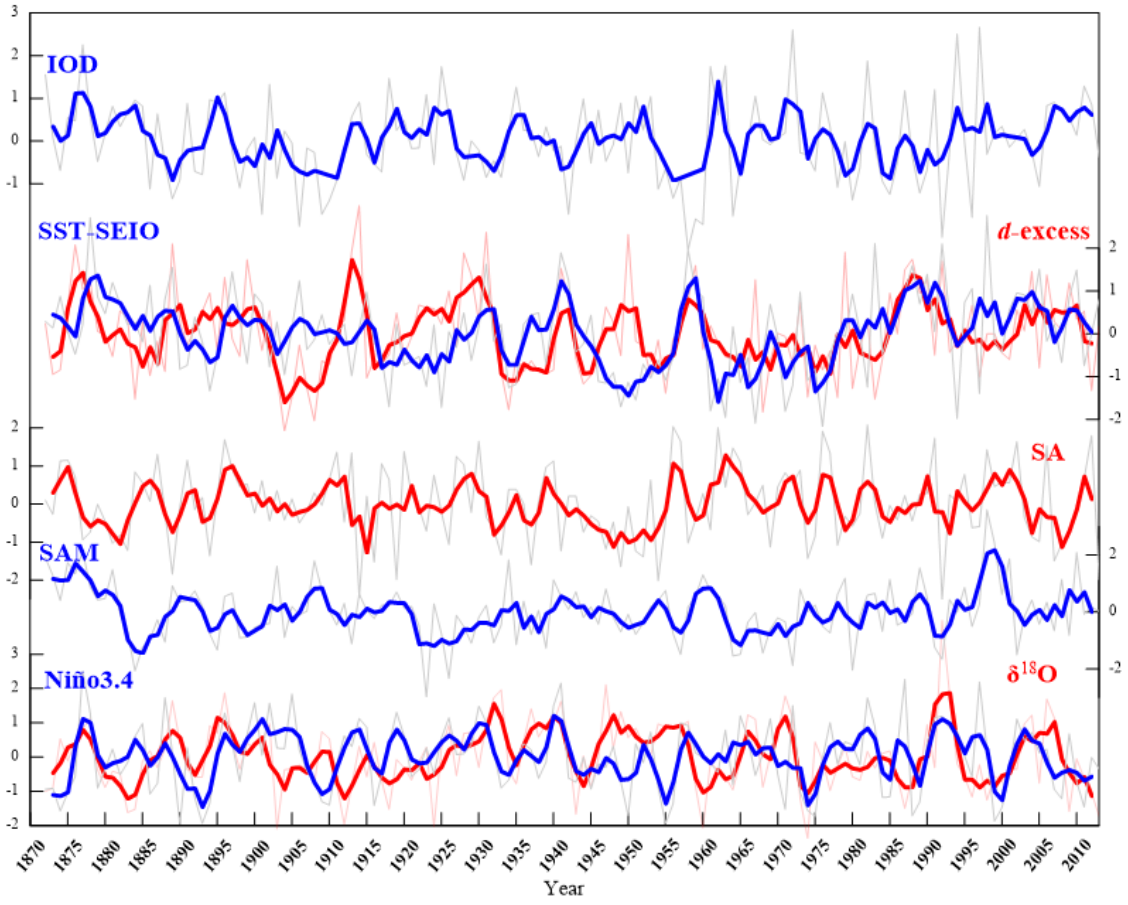


Figure 4. Comparison of the standardized profiles (thin lines) for detrended time series of SA, $\delta^{18}O$, and *d*-excess with the IOD, SST anomaly of the southeastern Indian Ocean (SST-SEIO), SST anomalies over the Southern Hemisphere, the SAM, and Nino3.4 for 1872–2013 CE. The thick lines (blue and red) indicate the 3-year running average

REPLY TO THE COMMENTS BY REVIEWER #1

General comment: The manuscript by Nyamgerel et al investigates climate related signals in the GV7-C ice core located in East Antarctica, and the potential teleconnections between the tropics and Antarctica. While the manuscript addresses an important question regarding the climate variability signals within the GV7-C ice core in East Antarctica, major revisions are necessary before it can be considered for publication.

Answer: We sincerely appreciate the reviewer's evaluation and constructive feedback. In response to the major revision request, we have carefully revised the manuscript. Please kindly see the detailed responses provided below

My main concerns that need to be addressed before further review are:

Comment 1: (1) Additional detail added to the method. Currently the method lacks sufficient detail to understand and have confidence in the results and interpretation. My key concerns include:

- No information is provided on important data processing and statistical information, including any detrending of dataset or consideration of how trends influence correlation results, statistical tests used for significance, consideration of autocorrelation and degrees of freedom on significance.

Answer: We sincerely appreciate the reviewer's comment highlighting the need for clearer statistical description and methodological transparency. In response, we have revised the entire Section 2.3 (Climate data and analysis) to explicitly describe data preprocessing and statistical procedures as following.

We improved the description about data distribution and linearization, detrending. The analyses are conducted on annual means of the ice core and climate data. Annual averaging reduces the influence of seasonal extreme values. For the ice core records, depending on the resolution of the records (3–21 data points per year), we were not able obtain continuous seasonal values. For the climate data, we tested/examined at both annual and seasonal (DJF, MAM, JJA, SON) scales to assess potential relationships. Overall patterns and physical interpretations were consistent when annual means were used; therefore, annual values of the climate data were used in the correlation analysis.

We have considered detrending on the time series, in the correlation analyses, we conducted on the original and linearly detrended (removed linear trends to compare the fluctuations in the ice core and climate data) time series of the ice core and climate data, and the results are described in Sections 3.3.1 – 3.3.2. We have also conducted the correlation analysis on annual and three-year running averages. The correlation analysis on the smoothed time series (three-year running averages) were conducted to reduce stratigraphic noise, and at least three-year averaging also has been suggested for obtaining a significant climatic signal from the GV7 site (e.g., Frezzotti et al., 2007; Khan et al., 2021; Schlosser and Oerter, 2002). Pearson correlation coefficients were calculated and their significance was assessed using a two-tailed Student's t-test with corresponding *p*-values.

We also considered the effect of autocorrelation, although, the ice core and climate data were annually averaged and linear trends were removed. The effects of autocorrelation on the correlation analysis were tested using effective number of degrees of freedom (N_{eff}) (at $p < 0.05$) (Bretherton et al., 1999). The results indicated negligible autocorrelation effects on the reported correlations (for the

correlation coefficients in Tables 4 and 6), and thus the correlations can be considered statistically robust. We have added the results (Neff ≈ N, indicating negligible autocorrelation effects with p values) for each correlation coefficients, and mentioned the autocorrelation effects in the materials and method section of the revised manuscript.

Table 4. Pearson's correlation coefficients (r) between the GV7-C ice core records and the climate variables for the period 1957–2013 CE. Correlations are calculated for annual data and three-year running averages in the detrended and original time series (shown in parentheses). Larger values ($r > 0.3$ at $p < 0.05$) are marked in bold. SIE (EA) and SIE (RA) denotes sea ice extent over East Antarctica and the Ross-Amundsen Sea sector.

	IOD	SST (SEIO)	SAM	SOI	Niño3.4	SIE (EA)	SIE (RA)
Annual average							
SA	**0.37** (0.28) Neff ≈ N, indicating negligible autocorrelation effects, at p < 0.001	–0.22 (–0.26)	0.12 (0.04)	–0.00 (–0.01)	0.04 (0.04)	0.01 (–0.02)	0.09 (0.00)
$\delta^{18}O$	–0.01 (–0.03)	–0.06 (–0.07)	–0.18 (–0.18)	–0.26 (-0.26)	0.22 (0.22)	–0.06 (–0.07)	–0.23 (–0.22)
d-excess	–0.19 (–0.07)	0.25 **(0.33)**	–0.03 (0.09)	0.02 (0.03)	0.04 (0.05)	–0.05 (0.02)	0.11 (0.22)
Three-year running average							
SA	**0.39** (0.18) Neff ≈ N, indicating negligible autocorrelation effects, at p < 0.0001	**–0.30 (–0.36)** Neff ≈ N, indicating negligible autocorrelation effects, at p < 0.05	0.11 (–0.06)	0.09 (0.09)	–0.11 (–0.14)	0.11 (0.04)	–0.18 (–0.02)
$\delta^{18}O$	–0.06 (–0.02)	0.02 (0.04)	**–0.41** (–0.27) Neff ≈ N, indicating negligible autocorrelation effects, at p < 0.0017	**–0.49 (–0.49)** Neff ≈ N, indicating negligible autocorrelation effects, at p < 0.0001	**0.46 (0.46)** Neff ≈ N, indicating negligible autocorrelation effects, at p < 0.0004	–0.14 (–0.11)	**–0.47 (–0.32)** Neff ≈ N, indicating negligible autocorrelation effects, at p < 0.0002
d-excess	**–0.45** (–0.06) Neff ≈ N, indicating negligible autocorrelation effects, at p < 0.0005	**0.64 (0.72)** Neff ≈ N, indicating negligible autocorrelation effects, at p < 0.0001	–0.15 (–0.21)	–0.11 (–0.09)	0.24 (0.27)	**–0.35** (–0.16) Neff ≈ N, indicating negligible autocorrelation effects, at p < 0.0092	0.01 (0.31)

Table 6. Pearson's correlation coefficients (r) between the GV7-C ice core records and the climate variables for the period 1872–2013 CE. Correlations are calculated for annual data and three-year running averages in the detrended and original time series (shown in parentheses). Larger values ($r > 0.3$ at $p < 0.05$) are marked in underlined bold.

	IOD	SST (SEIO)	SST anomaly	SAM	Niño3.4
Annual average					
SA	0.10 (0.10)	–0.15 (–0.11)	–0.03 (–0.01)	0.03 (0.03)	0.02 (0.02)

$\delta^{18}O$	–0.04 (–0.04)	–0.01 (–0.02)	–0.10 (–0.08)	–0.16 (–0.14)	0.14 (0.13)
d-excess	–0.02 (0.08)	0.02 (0.28)	–0.20 (0.28)	0.06 (0.18)	0.12 (0.13)
Three-year running average					
SA	–0.04 (0.01)	–0.02 (0.02)	–0.04 (0.02)	0.00 (0.04)	0.02 (0.03)
$\delta^{18}O$	–0.12 (–0.11)	0.00 (–0.02)	–0.13 (–0.11)	–0.23 (–0.16)	0.19 (0.18)
	0.03 (0.23)	**0.32 (0.43)**	0.26 **(0.39)**	–0.02 (0.24)	0.24 (0.26)
d-excess		Neff ≈ N, indicating negligible autocorrelation effects, at p < 0.00017			

We have excluded the correlation results on 5-year running averaged as well as 3- and 5-year (point) averages in the revised version, which we considered as unnecessary details. We have revised Section 2.3 as shown below.

"2.3 Climate data and analysis

The $\delta^{18}O$ ($\delta^{18}O$ is preferred because it is highly correlated with δD; r = 0.99), d-excess, and SA from the GV7-C ice core were used in the correlation analysis. Two time periods (1957–2013 CE and 1872–2013 CE) were selected for correlation analyses between GV7-C records and climate variables based on data availability (e.g., SAM indices) and to ensure adequate sample size. The annual means of the ice core records derived from multiple intra-annual samples (3–21 data points per year; average 8) were used in the correlation analysis, which reduces the influence of seasonal extreme values. Because isotopic composition recorded in an annual layer reflects integrated snowfall through the year, GV7-C records represent the combined influence of seasonal processes. For the climate data, we therefore examined at both annual (January–December) and seasonal (DJF, MAM, JJA, SON) scales to assess potential relationships. Although some seasonal differences were observed, overall patterns and physical interpretations were consistent when annual means were used; therefore, annual values are presented to represent the net integrated climate signal preserved in the ice core. Correlation analyses were conducted on original and linearly detrended time series (annual and three-year running averages) of the ice core and climate data, and the results are described in Sections 3.3.1 – 3.3.2. The correlation analysis on the smoothed time series were conducted to reduce stratigraphic noise, and at least three-year averaging has been suggested for obtaining a significant climatic signal from the GV7 site (e.g., Frezzotti et al., 2007; Khan et al., 2021; Schlosser and Oerter, 2002). Pearson correlation coefficients were calculated and their significance was assessed using a two-tailed Student's t-test with corresponding p-values. Although, the ice core and climate data were annually averaged and linear trends were removed, the effects of autocorrelation on the correlation analysis were tested using effective number of degrees of freedom (N_{eff}) (at p < 0.05) (Bretherton et al., 1999). The results indicated negligible autocorrelation effects on the reported correlations (for the correlation coefficients in Tables 4 and 6), and thus the correlations can be considered statistically robust.

For the 1957–2013 CE period, the following climate indices were compared with the annual means of the GV7-C ice core records: station-based SAM index (Marshall G and National Center for Atmospheric Research Staff, 2018), the Southern Oscillation Index (SOI) (https://www.ncei.noaa.gov/access/monitoring/enso/soi), Niño3.4 index (https://psl.noaa.gov/gcoswgsp/Timeseries/Nino34), Indian Ocean Dipole (IOD) index representing the SST gradient between the western and southeastern equatorial IO

(https://psl.noaa.gov/gcos_wgsp/Timeseries/DMI), SST anomaly in the southeastern IO (SST-SEIO) (https://psl.noaa.gov/gcos_wgsp/Timeseries/DMI), and reconstructed sea ice extent (SIE) over the Ross–Amundsen Sea sector (162°E–250°E) and the East Antarctic sector (71°E–162°E) (Fogt et al., 2023). Moreover, for the 1957–2013 CE period, spatial correlation analyses (at 95% confidence interval) were conducted between annual GV7-C records and gridded ERA5 reanalysis data (air temperature, SST, sea ice concentration [SIC], 10-m wind speed, zonal [u] and meridional [v] wind components, and total precipitable water) using Climate Reanalyzer developed by the University of Maine, USA (https://climatereanalyzer.org/). Since ice-core isotopic signals reflect a broad range of thermodynamic and dynamic influences, spatial correlation analyses were conducted for physically plausible scenarios to help identify potential moisture supply regions over a longer time period (1957–2013 CE) than previous studies (Caiazzo et al., 2017; Khan, 2019). Spatially coherent and physically interpretable patterns are selectively presented and used as supportive evidence in the interpretation of climate-related signals from the GV7-C ice core. Principal component analysis (PCA), a linear dimensionality reduction technique, was employed to investigate potential similarities in variability between the annual means of the ice-core records and seasonal and annual means of climate datasets (IOD, SST-SEIO, SAM, SOI, Niño3.4, SIE) for 1957–2013 CE. The PCA results conducted on annual mean values were selected and presented in this study. For the 1872–2013 CE period, the GV7-C ice core data were compared with the IOD index, SST-SEIO, reconstructed SST anomaly over the Southern Hemisphere (https://www.ncei.noaa.gov/access/monitoring/climate-at-a-glance/global/time-series) (Huang et al., 2017), reconstructed SAM index (https://psl.noaa.gov/data/20thC_Rean/timeseries/monthly/SAM), and Niño3.4. SAM and ENSO are considered key modes potentially affecting Antarctic climate variability (Turner et al., 2009; Cohen et al., 2012; Pohl et al., 2021; Wille et al., 2021), and the SOI and Niño3.4 indices describe Pacific variability that can influence the climate of the Southern Ocean and Antarctica (Meyerson et al., 2002; Bertler et al., 2004). Moreover, the temperature anomalies (IOD index, SST-SEIO) over the Indian Ocean affects the air temperature (Zhang and Duan, 2023), sea ice extent (Kim et al., 2023; Zhang et al., 2024) and precipitation in Antarctica (Lee et al., 2024)."

- Limited or no consideration of the physical mechanisms for how climate variability modes influence Antarctic weather and climate and how that is reflected in the method.

    1. For example, for ENSO if the annual period used is January to December (not specified in the manuscript), this splits ENSO events in half (which usually run from austral winter through to late austral summer) and is not related to the physical process that links ENSO variability to the Antarctic climate via Rossby wave train, and how this interacts with the phase of SAM and in different seasons.
    2. Considerations required for IOD include phase lock (e.g. the influence of IOD on southern hemisphere climate is phase locked by the arrival of the southern monsoon in the southern hemisphere and is usually only active between austral winter and early summer) and the seasons when the Rossby wave teleconnection to Antarctic climate is possible and not reflected by the interactions with the polar jet.
    3. SAM considerations – asymmetric vs symmetric component, and how SAM interacts with weather systems in the region that influence ice core interpretation.

Answer: Thank you for the helpful comment. Since the ice core signals reflect broad range of processes, with the GV7-C ice core data (one of the high SA, well-dated, high-resolution data), we have considered both annual and seasonal characteristics of the climate modes, and tested the analysis (correlation, PCA analysis) on multiple cases (can be said many) at initial steps. We tested seasonal values and found no significant deviations when using annual values instead of seasonal

values, we then selected annual values. We have mentioned “Jan to Dec” for annual period in the materials and method section.

We agree on the importance regarding the physical mechanisms linking large-scale climate modes to Antarctic climate variability. ENSO, IOD, and SAM exhibit strong seasonal characteristics and influence Antarctic climate through seasonally dependent dynamical pathways. Because ice-core isotopic records represent the integrated precipitation signal accumulated throughout the year, the annual layer reflects the combined influence of seasonal processes rather than a single seasonal state. For this reason, we initially tested both seasonal (DJF, MAM, JJA, and SON) and annual correlations in the exploratory phase of the analysis. While some seasonal differences were observed, the overall patterns of association and physical interpretation remained consistent when annual means were used. Therefore, annual (January to December) values were selected to represent the net integrated climate signal recorded in the GV7-C ice core. We acknowledge that ENSO events often span austral winter through late austral summer and that IOD variability is phase-locked to austral winter–spring conditions. However, because the isotopic composition recorded in each annual layer reflects snowfall accumulated across multiple seasons, annual averaging is appropriate for capturing the integrated teleconnection signal.

To clarify this methodological reasoning, we have stated in Section 2.3 that climate data were examined on both annual (January to December) and seasonal (DJF, MAM, JJA, SON) scales prior to selecting the annual representation. This clarification has been added to improve transparency regarding the physical interpretation underlying the methodological design.

“2.3 Climate data and analysis

The $\delta^{18}O$ ($\delta^{18}O$ is preferred because it is highly correlated with δD; r = 0.99), d-excess, and SA from the GV7-C ice core were used in the correlation analysis. Two time periods (1957–2013 CE and 1872–2013 CE) were selected for correlation analyses between GV7-C records and climate variables based on data availability (e.g., SAM indices) and to ensure adequate sample size. The annual means of the ice core records derived from multiple intra-annual samples (3–21 data points per year; average 8) were used in the correlation analysis, which reduces the influence of seasonal extreme values. Because isotopic composition recorded in an annual layer reflects integrated snowfall through the year, GV7-C records represent the combined influence of seasonal processes. For the climate data, we therefore examined at both annual (January–December) and seasonal (DJF, MAM, JJA, SON) scales to assess potential relationships. Although some seasonal differences were observed, overall patterns and physical interpretations were consistent when annual means were used; therefore, annual values are presented to represent the net integrated climate signal preserved in the ice core. Correlation analyses were conducted on original and linearly detrended time series (annual and three-year running averages) of the ice core and climate data, and the results are described in Sections 3.3.1 – 3.3.2. The correlation analysis on the smoothed time series were conducted to reduce stratigraphic noise, and at least three-year averaging has been suggested for obtaining a significant climatic signal from the GV7 site (e.g., Frezzotti et al., 2007; Khan et al., 2021; Schlosser and Oerter, 2002). Pearson correlation coefficients were calculated and their significance was assessed using a two-tailed Student’s t-test with corresponding p-values. Although, the ice core and climate data were annually averaged and linear trends were removed, the effects of autocorrelation on the correlation analysis were tested using effective number of degrees of freedom (N_{eff}) (at $p < 0.05$) (Bretherton et al., 1999). The results indicated negligible autocorrelation effects on the reported correlations (for the correlation coefficients in Tables 4 and 6), and thus the correlations can be considered statistically robust.

For the 1957–2013 CE period, the following climate indices were compared with the annual means of the GV7-C ice core records: station-based SAM index (Marshall G and National Center for Atmospheric Research Staff, 2018), the Southern Oscillation Index (SOI) (https://www.ncei.noaa.gov/access/monitoring/enso/soi), Niño3.4 index (https://psl.noaa.gov/gcoswgsp/Timeseries/Nino34), Indian Ocean Dipole (IOD) index representing the SST gradient between the western and southeastern equatorial IO (https://psl.noaa.gov/gcos_wgsp/Timeseries/DMI), SST anomaly in the southeastern IO (SST-SEIO) (https://psl.noaa.gov/gcos_wgsp/Timeseries/DMI), and reconstructed sea ice extent (SIE) over the Ross–Amundsen Sea sector (162°E–250°E) and the East Antarctic sector (71°E–162°E) (Fogt et al., 2023). Moreover, for the 1957–2013 CE period, spatial correlation analyses (at 95% confidence interval) were conducted between annual GV7-C records and gridded ERA5 reanalysis data (air temperature, SST, sea ice concentration [SIC], 10-m wind speed, zonal [u] and meridional [v] wind components, and total precipitable water) using Climate Reanalyzer developed by the University of Maine, USA (https://climatereanalyzer.org/). Since ice-core isotopic signals reflect a broad range of thermodynamic and dynamic influences, spatial correlation analyses were conducted for physically plausible scenarios to help identify potential moisture supply regions over a longer time period (1957–2013 CE) than previous studies (Caiazzo et al., 2017; Khan, 2019). Spatially coherent and physically interpretable patterns are selectively presented and used as supportive evidence in the interpretation of climate-related signals from the GV7-C ice core. Principal component analysis (PCA), a linear dimensionality reduction technique, was employed to investigate potential similarities in variability between the annual means of the ice-core records and seasonal and annual means of climate datasets (IOD, SST-SEIO, SAM, SOI, Niño3.4, SIE) for 1957–2013 CE. The PCA results conducted on annual mean values were selected and presented in this study. For the 1872–2013 CE period, the GV7-C ice core data were compared with the IOD index, SST-SEIO, reconstructed SST anomaly over the Southern Hemisphere (https://www.ncei.noaa.gov/access/monitoring/climate-at-a-glance/global/time-series) (Huang et al., 2017), reconstructed SAM index (https://psl.noaa.gov/data/20thC_Rean/timeseries/monthly/SAM), and Niño3.4. SAM and ENSO are considered key modes potentially affecting Antarctic climate variability (Turner et al., 2009; Cohen et al., 2012; Pohl et al., 2021; Wille et al., 2021), and the SOI and Niño3.4 indices describe Pacific variability that can influence the climate of the Southern Ocean and Antarctica (Meyerson et al., 2002; Bertler et al., 2004). Moreover, the temperature anomalies (IOD index, SST-SEIO) over the Indian Ocean affects the air temperature (Zhang and Duan, 2023), sea ice extent (Kim et al., 2023; Zhang et al., 2024) and precipitation in Antarctica (Lee et al., 2024)."

- Consideration of data reliability (e.g. ERA5 data reliability prior to 1979 in the Southern Hemisphere has been highlighted as having issues and artificial trends due to limited data prior to satellites). Reanalysis that considers only pressure (e.g. 20th century reanalysis) have been shown to be more reliable as they have less step changes in the number and type of observation used in data assimilation.

Answer: We appreciate the comment and agree on the careful consideration of reanalysis data. We acknowledge that the analysis included in this study was initiated and driven by previous studies at this site that mentioned the influences of climate indices (e.g., ENSO, SAM, SOI), but were based on relatively shorter records (mostly since 1979). We expanded the comparison with reanalysis data to test and obtain supporting confirmation from spatial correlations, since the ice core isotopic signals reflect a broad range of influencing factors. The purpose was to support the assumptions and identification of the moisture supply region from the perspective of spatial relevance over a relatively longer time period (1957–2013 CE) than previous studies (Caiazzo et al., 2017; Khan, 2019). The results were used as support in the interpretation based on the spatial correlation maps with ERA5

reanalysis. The identification of positive and negative correlations, the regions exhibiting these correlations, and the relevant seasons (where possible) were considered to support the interpretation; the interpretations are not based solely on ERA5 spatial correlation analysis. Within the scope of the study, we checked the spatial correlation maps, and we agree that it is possible and worthwhile to expand the data selection and analyses in greater detail (e.g., using 20th century analysis) in future studies. Alternative reanalysis products may offer complementary perspectives, and such comparisons represent a valuable direction for future research. We have revised Section 2.3 to explicitly state that spatial correlation analyses using ERA5 are used as supportive evidence and that interpretations are not based solely on reanalysis-derived fields.

"Since ice-core isotopic signals reflect a broad range of thermodynamic and dynamic influences, spatial correlation analyses were conducted for physically plausible scenarios to help identify potential moisture supply regions over a longer time period (1957–2013 CE) than previous studies (Caiazzo et al., 2017; Khan, 2019). Only spatially coherent and physically interpretable patterns are selectively presented and used as supportive evidence in the interpretation of climate-related signals from the GV7-C ice core."

Limited details provided on the principle component analysis method and results.

Answer: We thank for pointing out the need for clearer methodological detail regarding the principal component analysis. In response, we have expanded the description of the PCA procedure in Section 2.3 and clarified the interpretation of the results in Section 3.3.1.

Specifically, we now state that all variables included in the PCA were standardized to zero mean and unit variance prior to analysis to ensure comparability among datasets with different units and magnitudes. The PCA was conducted based on the correlation matrix, and components with eigenvalues greater than 1 were retained following the Kaiser criterion. No rotation was applied, as the objective was to identify the dominant modes of joint variability rather than to maximize separation between components.

In addition, we have revised Section 3.3.1 to clarify the physical interpretation of the principal components and to explicitly present the loading matrix (correlation coefficients at $p < 0.05$) in Table 5. The variance explained by each principal component and the cumulative variance are now clearly reported. The revised text emphasizes that PCA results are interpreted in terms of coherent thermodynamic and dynamic variability patterns rather than as evidence of direct causality. We believe these revisions improve the transparency and robustness of the PCA methodology and clarify how the results support the overall interpretation of climate-related signals in the GV7-C ice core.

To address this point, we expanded the PCA description in Sect. 2.3 and clarified the interpretation of the PCA loadings in Sect. 3.3.1. We also included SST-SEIO among the PCA variables to align with the correlation analysis for 1957–2013 CE. The revised text is provided below.

Section 2.3 Climate data and analysis: *"Principal component analysis (PCA), a linear dimensionality reduction technique, was employed to investigate potential similarities in variability between the annual means of the ice-core records and seasonal and annual means of climate datasets (IOD, SST-SEIO, SAM, SOI, Niño3.4, SIE) for 1957–2013 CE. The PCA results conducted on annual mean values were selected and presented in this study."*

Section 3.3.1 Climate signals for the 1957–2013 CE period:

"PCA analysis conducted for 1957–2013 CE, with the loading matrix (correlation coefficients at $p < 0.05$) presented in Table 5. Principal component (PC) 1 clustered $\delta^{18}O$, the SAM, SOI, Niño3.4, and SIE over the East Antarctica and Ross-Amundsen Sea region. This reflected the importance of both thermodynamic and dynamic effects on the decrease (increase) in $\delta^{18}O$ with an increase (decrease) in the SIE, stronger (weaker) westerly winds (i.e., the SAM and SOI), and lower (higher) SSTs in the Niño3.4 region. In PC 2, d-excess and SA were clustered with IOD, SAM, SIE, and particularly strong signal of SST-SEIO. This can represent the increasing (decreasing) d-excess with increased (decreased) evaporation with warm (cold) SSTs particularly over the southeastern IO. Moreover, there could be a weak relevance with enhanced (weakened) air mass transport with strong westerlies (i.e., the SAM), consequent wind-induced increase (decrease) in SIE over East Antarctica and relatively cooler temperature over the eastern IO (decreasing IOD). It is ambiguous to explain the negative correlation between the SA and SST-SEIO in PC 2. However, PC 3 included SA only, with more stronger signals of IOD, SAM, SOI, Niño3.4 and SIE over the East Antarctica. This can represent the thermodynamic effects on SA with increased (decreased) evaporation with warm SSTs over western equatorial IO and central tropical PO (i.e., the SOI and Niño3.4), enhanced moisture transport with strong westerlies (i.e., the SAM), and the wind-induced SIE over East Antarctica. PC 4 was characterized by an increasing (decreasing) $\delta^{18}O$, d-excess with decreasing (increasing) SST-SEIO which can be explained by the intrusion of different air masses with evident d-excess signals together with $\delta^{18}O$. Overall, PCA classified the variables into species representing the climatic signals corresponding to the PO (PC 1) and southeastern IO sector of the Southern Ocean (PC 2). Interestingly, the relatively strong detectability of the thermodynamic effect on d-excess, which is induced by the IO sector, likely to indicate the significant (detectable) temperature signals in this region."

Table 5. Loadings of the variables for the first four principal components (PCs) of the PCA analysis conducted with the data for 1957–2013 CE. Larger values of correlation coefficients ($r > 0.3$, at $p < 0.05$) are marked in underlined bold.

Variables	PC1	PC2	PC3	PC4
SA	0.04	**–0.48**	**0.43**	–0.04
$\delta^{18}O$	**–0.39**	0.20	–0.04	**0.77**
d-excess	0.05	**0.63**	–0.07	**0.49**
IOD	0.12	**–0.30**	**0.77**	0.27
SST-SEIO	–0.07	**0.82**	–0.08	**–0.40**
SAM	**0.52**	**0.30**	**0.56**	–0.08
SOI	**0.82**	–0.23	**–0.43**	0.13
Niño3.4	**–0.80**	0.27	**0.47**	–0.13
SIE (EA)	**0.52**	**0.31**	**0.38**	0.00
SIE (RA)	**0.84**	0.29	0.13	0.05
Variance explained (%)	*27*	*18*	*17*	*11*
Cumulative percent (%)	*27*	*45*	*62*	*73*

- Multiple correlations are calculated which increases the type-1 error (i.e. increased chance of false positives). How is this being considered?

Answer: We agree that conducting many correlation tests can increase the chance of false positives. The correlation analyses were largely hypothesis-driven, motivated by prior work at GV7 and nearby sites, and the spatial correlation maps are used as supporting evidence to evaluate whether the inferred relationships are geographically coherent and physically plausible over 1957–2013 CE. The

correlations are interpreted conservatively, with emphasis on effect size, temporal persistence, and physical consistency, and p-values.

Comment 2: (2) Most of the figures are in the supplementary material. These are referred to in the results and essential to be able to understand the results and interpretation discussed so need to be made more concise to be able to be included in the main text.

Answer: Thank you for this clear comment. As we have changed the manuscript structure according to the other comments, the figures in the supplementary material were generated by the spatial correlation analysis with ERA5 reanalysis, as a supportive results to the main interpretations (section 3.3.1. and 3.3.2) of the manuscript. The description of the figures moved to section 3.2. (Spatial correlation analysis with ERA5 reanalysis). We included information in materials and method section *(2.3. Climate data and analysis)*, as it shown below.

"Since ice-core isotopic signals reflect a broad range of thermodynamic and dynamic influences, spatial correlation analyses were conducted for physically plausible scenarios to help identify potential moisture supply regions over a longer time period (1957–2013 CE) than previous studies (Caiazzo et al., 2017; Khan, 2019). Only spatially coherent and physically interpretable patterns are selectively presented and used as supportive evidence in the interpretation of climate-related signals from the GV7-C ice core."

Moreover, we removed Supplementary Figures 9 and 10 because they described widely known relationships between climate variables and Niño 3.4 and SAM, rather than relationships specific to the GV7-C ice core.

We revised Sect. 3.2. (Spatial correlation analysis with ERA5 reanalysis) to improve clarity and to make the supporting figures more concise. The spatial-correlation results are now consolidated and presented as three combined figures in the Supplement (Figs. S1–S3), which summarize the key, physically interpretable patterns used in our discussion. The revised text for Sect. 3.2.2 is provided below.

"3.2 Spatial correlation analysis with ERA5 reanalysis

Spatial correlation analyses (95% confidence interval) were conducted between annual GV7-C records ($\delta^{18}O$, d-excess, and SA) and annual/seasonal ERA5 reanalysis fields for 1957–2013 CE to explore potential spatial patterns consistent with moisture supply and transport pathways. Significant and physically interpretable patterns are selectively presented in the Supplement (Figs. S1–S3) and are used as supporting evidence in the discussion of likely source regions. For interpretation, the Pacific Ocean (PO) sector is defined here as the western Pacific (90–160°E), Ross Sea (160°E–130°W), and Amundsen–Bellingshausen Seas (130–60°W), while the Indian Ocean (IO) sector is defined as 20–90°E. Annual mean $\delta^{18}O$ shows positive correlations with 2 m air temperature and SST primarily over the PO sector (Fig. S1a, b). Positive relationships with air temperature (2 m and 850 hPa) and total column precipitable water are most evident during DJF over parts of the PO and IO sectors (Fig. S1d–f). Negative correlations are observed with sea ice concentration (SIC) over the Ross Sea region (Fig. S1c). Wind-speed correlations (10 m; annual and MAM) are generally negative (Fig. S1g, j), and zonal wind (u-wind) correlations highlight the belt of strong westerlies (Fig. S1h, k). The meridional wind (v-wind) correlations suggest a northward flow signature from the western PO sector and a southward flow signature from the IO sector during DJF (Fig. S1i), whereas these patterns weaken in MAM (Fig. S1l). Overall, $\delta^{18}O$ exhibits its clearest spatial coherence during DJF and MAM, consistent with the

seasonality of transport and snowfall in this coastal sector (Delmotte et al., 2000; Caiazzo et al., 2017). These patterns provide qualitative support for a relatively stronger PO-sector influence on $\delta^{18}O$ at GV7-C during DJF–MAM, although the overall relationships remain modest.

Annual mean d-excess exhibits positive correlations with air temperature (2 m and 850 hPa) over both the western PO and IO sectors (Fig. S2a–c). Temperature correlations in the IO sector are particularly evident in SON (Fig. S2c), whereas the d-excess response to temperature appears weaker in DJF (not shown). Correlations with SST (SON), SIC (JJA), and total column precipitable water (annual) further support a contribution of air masses from the IO sector and western PO to the GV7 region (Fig. S2d–f). In contrast to $\delta^{18}O$, correlations with wind speed and wind direction are relatively weak, except for a positive correlation with 10 m wind speed in some regions (Fig. S2g). The v-wind pattern indicates a southward flow signature from the IO sector and a northward flow signature in the western PO sector (Fig. S2i). Taken together, these spatial patterns suggest that thermodynamic source-region variability (e.g., SST/air-temperature conditions) may play a comparatively larger role for d-excess at GV7-C than do purely dynamical indicators, and they are consistent with a potentially important contribution from the IO sector, particularly during SON.

No clear and temporally consistent relationships are observed between SA and the investigated climate variables; only weak and spatially limited patterns are identified (Fig. S3). For example, SA shows weak negative correlations with 2 m temperature over parts of the Amundsen Sea coast and weak positive correlations with total column precipitable water offshore of the Ross Sea coast (Fig. S3a, b). SA also shows weak negative correlations with SIC over the Ross Sea region (Fig. S3c). Wind-speed correlations (10 m and 850 hPa) are weakly positive over parts of the PO sector (Fig. S3d, g), and the associated u- and v-wind patterns suggest modest transport signals (Fig. S3e, f, h, i). Overall, these results indicate that SA at GV7-C is likely influenced by multiple factors, including synoptic variability and transport efficiency, which may mask simple relationships with large-scale indices at annual resolution.

In sum, the results from the spatial correlation analysis suggest that the GV7-C ice core can be used to represent the regional climate conditions over the PO and IO sector. The correlations observed with $\delta^{18}O$ during the DJF and MAM seasons led us to consider the potential influence of the SAM. It is conceivable that a positive phase of SAM during the DJF and MAM seasons could strengthen the climate signals, allowing SAM-related signals to be detectable in $\delta^{18}O$ and SA during the 1957–2013 CE period. The dynamic influence of SAM can thus be important for $\delta^{18}O$ and SA, while d-excess is likely to represent thermodynamic changes over the IO and western PO sectors, particularly during the SON season. These correlations for d-excess can be remotely connected to the temperature variability over the tropical IO and PO (Masson-Delmotte et al., 2003).”

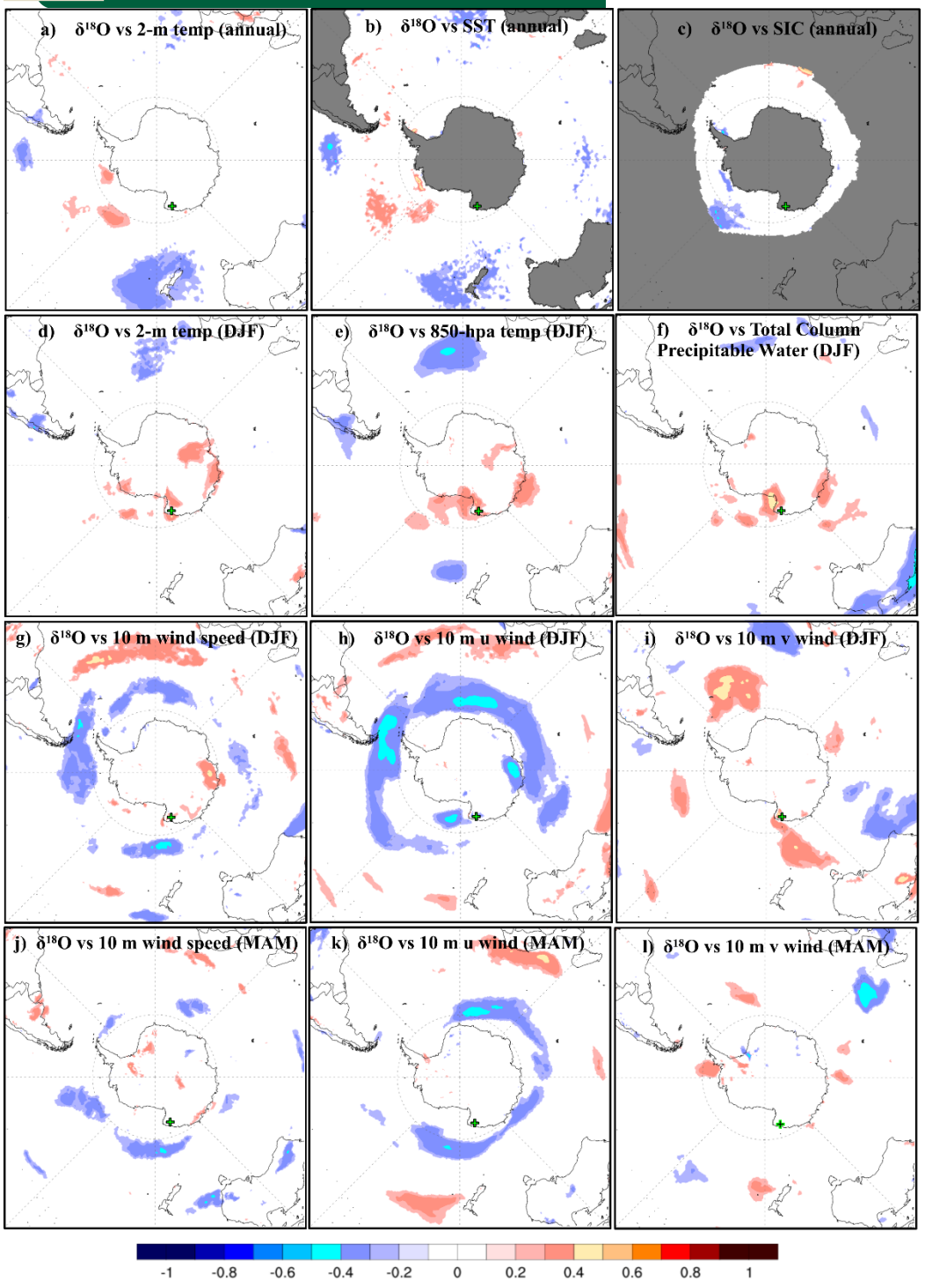


Figure S1. *Spatial correlation of $\delta^{18}O$ with (a, d, e) air temperature, (b) SST, and (c) SIC, (f) total column precipitable water, (g, j) wind speed, (h, k) u-wind components, and (i, l) v-wind components from the ERA5 reanalysis data for different seasons over the 1957–2013 CE period. The scale bars indicate Pearson's correlation coefficient (r) at $p < 0.05$. This figure was generated using Climate Reanalyzer (https://climatereanalyzer.org/) from the Climate Change Institute, University of Maine, USA.*

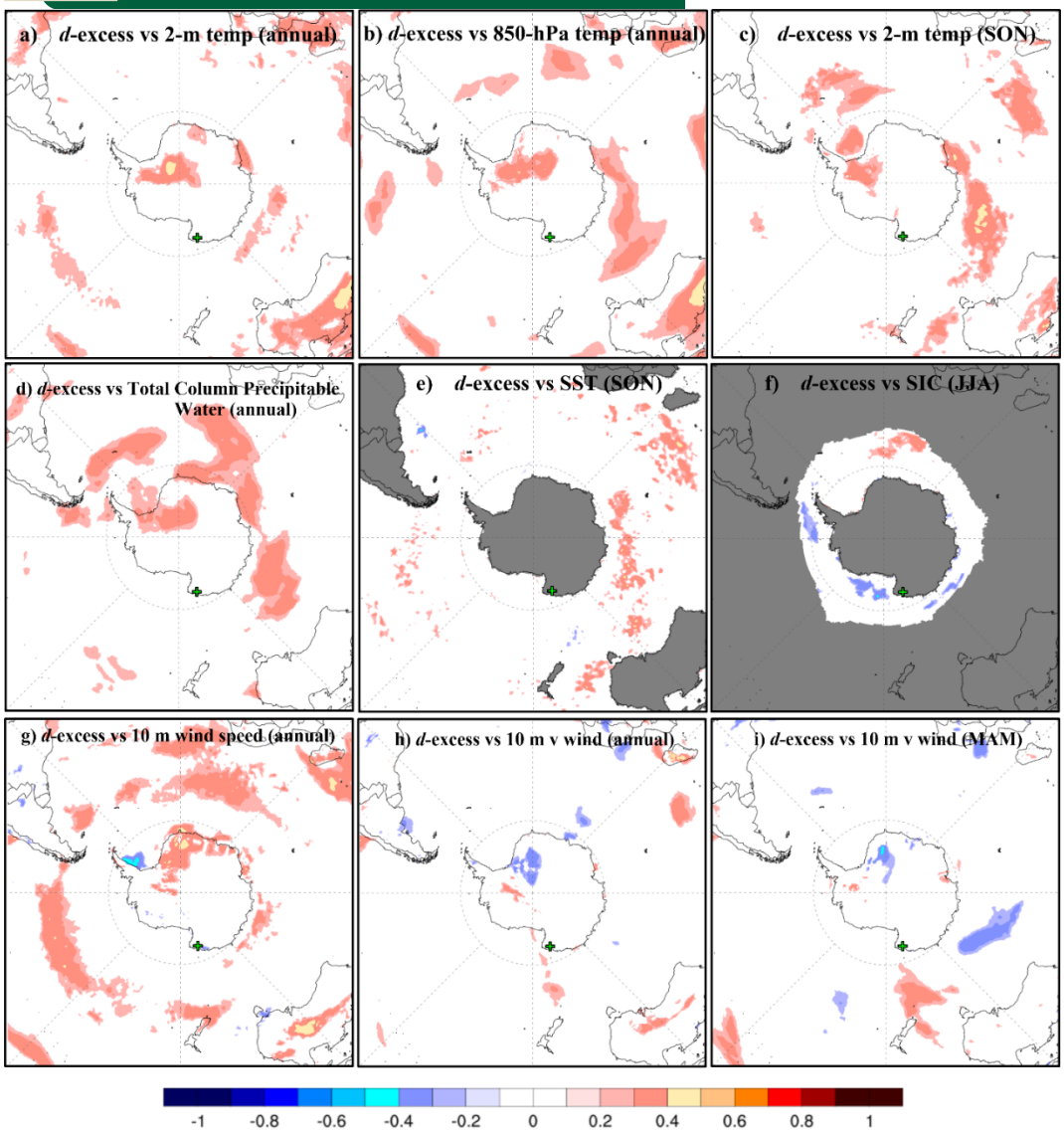


Figure S1. *Spatial correlation of d-excess with the (a, b, c) air temperature, (d) total column precipitable water, (e) SST, (f) SIC, (g) 10 m wind speed and (h, i) v-wind component from ERA5 reanalysis data for different seasons over the 1957–2013 CE period. The scale bars indicate Pearson's correlation coefficient (r) at p < 0.05. This figure was generated using Climate Reanalyzer (https://climatereanalyzer.org/) from the Climate Change Institute, University of Maine, USA.*

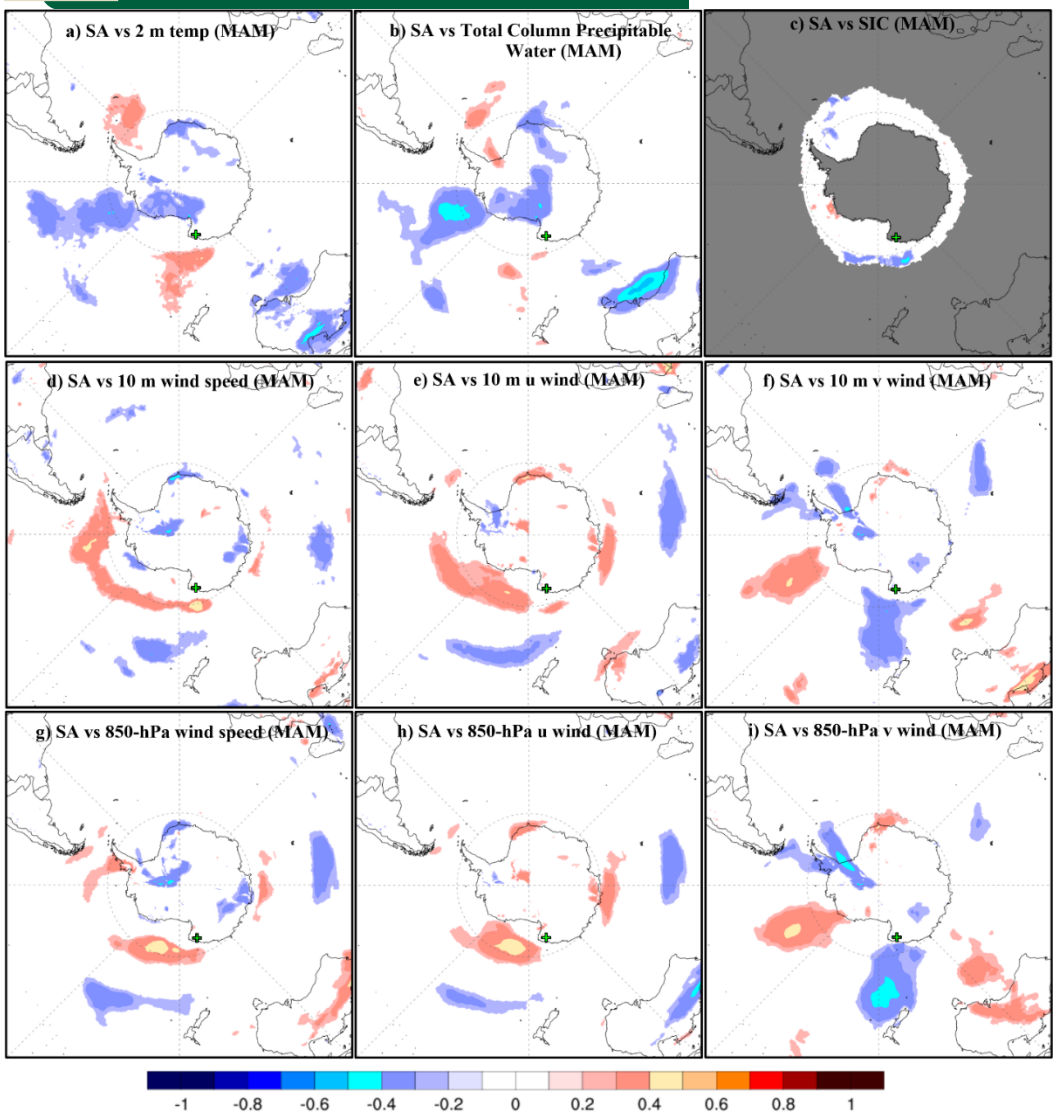


Figure S3. *Spatial correlation of SA with (a) air temperature, (b) total column precipitable water, (c) SIC, (d, g) 10 m wind speed, (e, h) u-wind components, and (f, i) v-wind components from ERA5 reanalysis data during the MAM season over the 1957–2013 CE period. The scale bars indicate Pearson's correlation coefficient (r) at $p < 0.05$. This figure was generated using Climate Reanalyzer (https://climatereanalyzer.org/) from the Climate Change Institute, University of Maine, USA.*

Comment 3: (3) Manuscript needs a major restructure. Currently there are a lot of discussion points in the results and it is challenging to determine what the key findings of the manuscript are. These need to be obvious based on the figures and results section, which is currently not the case with multiple figures in the supplementary and no clear structure to the result and discussion section.

Answer 3: Thank you for the clear comment that helped us to reconsider and re-organize the structure of the manuscript. We revised the structure of the manuscript. Duplications, unnecessary details in results, discussion, as well as in introducing sentences, have been edited (removed and edited concisely). We also edited/combined the interconnected results/duplicated but described separately as independent in the previous version.

Previous version	Edited version
3 Results 3.1 Characterization of the GV7-C ice core record 3.2 Relationship with climate variables during 1957–2013 3.2.1 Relationship with climate variables from ERA5 Reanalysis 3.2.2 Relationship with large-scale climate modes 3.3 Relationship with Long-Term Climate Modes 4 Discussion and implications	3 Results and discussion 3.1 Characterization of the GV7-C ice core record 3.2 Spatial correlation analysis with ERA5 reanalysis 3.3 Correlation analysis for 1957–2013 CE and 1872–2013 CE periods 3.3.1 Climate signals for the 1957–2013 CE period 3.3.2 Climate signals for the long-term records (1872–2013 CE) 3.4 Discussion and implications

We edited the captions of figures and tables, more clearly. We removed Supplementary Figures 9 and 10 because they described widely known relationships between climate variables and Niño 3.4 and SAM, rather than relationships specific to the GV7-C ice core.

We edited (removed duplications, re-organized the statements, highlighted key findings with supporting/relevant references) section 3.4 (Discussion and implications), abstract and conclusion, as it shown below.

"3.4 Discussion and implications

The variations in SA data from the GV7-C ice core showed significant interannual variations, and show only a weak correlation with IOD and SST-SEIO. The SA of the GV7-C ice core is assumed to be affected by the coupled influence of dynamic processes (i.e., the transport pathways and transport efficiency of moist air) or abrupt synoptic events (e.g., intense transport by atmospheric river events) (Turner et al., 2019; Wille et al., 2021). The variability in SA is affected by moisture transport via large-scale atmospheric circulation (Thomas et al., 2008; Udy et al., 2021; Cohen et al., 2012) and synoptic-scale short-lived events (e.g., atmospheric river events, atmospheric rivers) (Turner et al., 2019; Wille et al., 2021) and evident in the ice core records from coastal regions (Servettaz et al., 2020; Jackson et al., 2023). Moreover, the intensity and frequency of cyclone events also affect snowfall in Antarctic coastal areas (Dalaiden et al., 2020a). Particularly, in the Ross Sea region, the cyclonically driven SA is dominant and the region is sensitive to tropical and local climate drivers (Bertler et al., 2018). The contribution of synoptic-scale transport has been reported to be large for Victoria Land based on simulations over the 1985–2014 period (Dalaiden et al., 2020a). The influence of the ENSO on SA was evident at the Law Dome site (Roberts et al., 2015).

Based on the correlation of $\delta^{18}O$ in the GV7-C ice core with Nino 3.4, SOI, SAM, and SIE over the Ross-Amundsen Sea sector for 1957–2013 CE, the increasing (decreasing) $\delta^{18}O$ can be partly explained by the intrusion of relatively warm (colder) and moist (dry) air mass mainly through the PO sector of the Southern Ocean. This finding is comparable to other ice cores from the coastal Antarctica. In the Mount Brown South ice core in East Antarctica, evidence for moisture transport from the southern IO has been detectable from $\delta^{18}O$ signal, and the extreme precipitation events are linked with high-pressure systems in the mid-latitudes which increase the transport of warm and moist air mass from the southern IO (Jackson et al., 2023). In another ice core from Adélie Land covering the 1946–2006 CE

period, decadal variations in $\delta^{18}O$ and regional temperature were correlated (Goursaud et al., 2017). Moreover, $\delta^{18}O$ shows a tendency to decrease with increasing wind speed. However, the $\delta^{18}O$ on an annual scale could not be explained by changes in the SIE and temperature, indicating the importance of site-dependent climate signals in coastal ice cores (Goursaud et al., 2017). In another study, isotope-based results indicated colder SSTs, a higher SIE, stronger katabatic winds, and decreasing SA in the Victoria Low Glacier ice core during the 1288–1807 period (the Little Ice Age period) (Bertler et al., 2011). Little Ice Age-related cooling is also evident in the $\delta^{18}O$ signal from the Hercules Neve ice core for the 1770–1890 period (Stenni et al., 1999) and frequent cold intervals in the Talos Dome ice core (Stenni et al., 2002). In line with these observations, a slight decreasing trend was observed in the $\delta^{18}O$ signal from the GV7-C ice core during the 1782–1845 CE period (Fig. 4), which may be part of Little Ice Age cooling. After 1845, there was no long-term trend in $\delta^{18}O$ from the GV7-C ice core; rather, values lower than the long-term mean were frequently observed (the blue lines in Fig. 4). This depletion of $\delta^{18}O$ observed from the GV7-C ice core may be possibly linked with changes in atmospheric circulation (e.g., SAM-related cooling) (Thompson and Solomon, 2002). Moreover, in terms of temperature reconstruction, $\delta^{18}O$ signal in the GV7-C ice core contrasts to anthropogenic global warming, suggesting more local/regional variations or various climatic factors.

Based on the correlation of d-excess with SST-SEIO and SST anomaly (Tables 4 and 6), the d-excess signal from the GV7-C ice core likely to preserve the thermodynamic changes (i.e., SST changes) particularly over the IO sector of the Southern Ocean. Notably, the southern Indian Ocean exhibits the most intense cyclonic activity in the Southern Ocean, which may enhance the detectability of this signal in the d-excess record (Simmonds et al., 2003). D-excess as an indicator of climate conditions in the source region (Jouzel et al., 1982; Sodemann and Stohl, 2009; Lewis et al., 2013), warming over the Southern Ocean, was found to co-vary with higher d-excess in the Victoria Lower Glacier ice core (Bertler et al., 2011). At the Law Dome ice core site, d-excess also reflects SST changes over the southern IO sector (Masson-Delmotte et al., 2003). Particularly the abrupt increase in the d-excess in the 1970s was consistent with the d-excess of the GV7-C ice core. This relevance was explained by the abrupt changes in meridional atmospheric circulation, which led to the intrusion of warm subtropical moisture sources to the Antarctic coast during the 1970s (Masson-Delmotte et al., 2003). Consistently large peaks in the five-year running averaged time series for d-excess (both high and low values) were more frequent after 1845 (Fig. 2). Furthermore, it can be reported that the increasing phases in the global average temperature during the 1910–1945 CE period and since 1976 (IPCC, 2001) are evident in the increasing trend for d-excess (Fig. 2). Changes in the SAM have also been linked to tropical SST changes and other tropical variabilities (Clem and Fogt, 2013; Ding et al., 2012). The climate signals in some coastal sites, including RICE, Mt. Erebus Saddle, and Styx Glacier, have been thought to be primarily indicative of local and regional conditions in the Ross Sea region (Rhodes et al., 2012, Nyamgerel et al., 2020, 2024). Similarly, the influence IOD on the eastern East Antarctic precipitation was more dominant than the SAM-induced changes for the 1979–2014 (Lee and Jin, 2024). The IOD-related variation in the precipitation is explained by waves originating from the Indian Ocean that propagate southeastward, and inducing a low-pressure anomaly near eastern east Antarctica, consequently reducing precipitation. Thus, in the GV7-C ice core site, variabilities linked to remote teleconnections with SST over the IO sector of the Southern Ocean were assumed to be associated with d-excess.

Based on various correlation analysis with the climate variables used in this study, the following interpretations are summarized. During the period 1957–2013 CE, the correlation patterns based on SA, $\delta^{18}O$, and d-excess support that snow precipitating at the GV7-C site mainly originates from the Southern Ocean possibly via western PO and southeastern Indian Ocean. For the longer time scale (1872–2013), the correlation patterns based on d-excess for SST indicates more detectability of air mass intrusion from the Indian Ocean sector of the Southern Ocean. This suggests a warmer (colder)

ocean surface condition would be preserved in higher (lower) $\delta^{18}O$ (recent period) and d-excess values (recent and longer period) in the GV7-C ice core.

Lastly, it is notable that the importance of the GV7-C ice core records in climate studies. The historical temperature variability over the tropical ocean is important for global warming scenarios (IPCC, 2019). The projections show oceanic and atmospheric warming (Timmermann and Hellmer, 2013), and heat transported by the Southern Ocean further induces the melting of Antarctic ice shelves (Rignot et al., 2019). Particularly, the IO is experiencing the strongest and most robust warming (Du and Xie, 2008; Beal et al., 2019), largely driven by anthropogenic forcing (Dong et al., 2014), and it is projected to warm non-uniformly (Sharma et al., 2023). The IO and the PO temperature anomaly affects the surface air temperature of Antarctica (Zhang and Duan, 2023). Moreover, warm SSTs in the western tropical IO excite a poleward-moving Rossby wave, inducing the changes in sea ice extent (Zhang et al., 2024). The coastal and inland Antarctic regions emerge an anomalous retreat of sea ice extent and warming due to the short-term significant intrusion of warm and moist air masses associated with strong negative phase of SAM (Ionita et al., 2018). The SAM variation in the recent period is unprecedented in the last millennia (Fogt and Marshall, 2020) and the increasing influence of the SAM-ENSO coupling has been reported since the 1940s (in coastal Dronning Maud Land) (Ejaz et al., 2022). Thus, understanding the response of the Antarctic climate to ocean variability of the IO sector would be important."

Abstract. *Polar ice cores provide valuable archives of past climate variability, but interpreting these records in coastal East Antarctica remains challenging because multiple meteorological processes can influence the signals preserved in ice core. Here we investigate climate-related signals in the GV7-C ice core from East Antarctica (1782–2013 CE) using annual records of water isotopes ($\delta^{18}O$ and d-excess) and snow accumulation, by comparing them with large-scale climate indices and reanalysis-based climate data. Snow accumulation shows strong interannual variability, suggesting multiple and potentially competing controls, and is weakly linked to sea-surface temperature variability over the Indian Ocean Sector (1957–2013 CE). $\delta^{18}O$ exhibits relatively detectable relationships to Pacific-sector variability for 1957–2013 CE, whereas d-excess shows clearer relationships with sea-surface temperature variability in the Indian Ocean sector. Over the longer period (1872–2013 CE), $\delta^{18}O$ correlations generally weaken, implying time-varying controls, while d-excess retains persistent relationships, highlighting its utility for tracking moisture-source conditions. Overall, the GV7-C record suggests potential teleconnections between Antarctic coastal climate and tropical ocean variability.*

4 Conclusions

The $\delta^{18}O$, d-excess, and SA records from the GV7-C ice core in East Antarctica (1782–2013 CE) were analyzed to investigate potential links with large-scale climate variability. Snow accumulation shows significant interannual variability, likely reflecting the combined influence of transport pathways, synoptic events, and local processes, and is only weakly correlated with SST variability over the IO for 1957–2013 CE. In contrast, $\delta^{18}O$ and d-excess exhibit relatively detectable relationships with climate indices for 1957–2013 CE, including Niño3.4, SOI, SAM, IOD, SST-SEIO, and reconstructed sea ice extent over the Ross–Amundsen Sea sector and East Antarctic sector. Notably, d-excess shows a persistent relationship with SST-SEIO. Over the longer period (1872–2013 CE), $\delta^{18}O$ relationships generally weaken, suggesting time-varying controls, whereas d-excess retains correlations with SST-SEIO.

Correlation patterns and spatial analyses suggest that moisture reaching GV7-C primarily originates from the Southern Ocean, with contributions from the western Pacific and southeastern Indian Ocean sectors during 1957–2013 CE, while IO-sector influence is more evident over longer timescales. Overall, the GV7-C record provides evidence for potential teleconnections between low-latitude ocean variability and coastal East Antarctic climate.

Comment 4: (4) Missing key relevant references. One example is around the studies that investigate the link between weather regimes (including atmospheric rivers) and their links to modes of climate variability in the region, and how these influence the interpretation of climate signals in ice cores. Some relevant examples are:

- Synoptic Weather Types for the Ross Sea Region, Antarctica in: Journal of Climate Volume 26 Issue 2 (2013),
- Links between Large-Scale Modes of Climate Variability and Synoptic Weather Patterns in the Southern Indian Ocean in: Journal of Climate Volume 34 Issue 3 (2021),
- Relationship Between Weather Regimes and Atmospheric Rivers in East Antarctica - Pohl - 2021 - Journal of Geophysical Research: Atmospheres - Wiley Online Library,
- Antarctic Atmospheric River Climatology and Precipitation Impacts - Wille - 2021 - Journal of Geophysical Research: Atmospheres - Wiley Online Library
- The Dominant Role of Extreme Precipitation Events in Antarctic Snowfall Variability - Turner - 2019 - Geophysical Research Letters - Wiley Online Library

Given the above, I recommend major revisions to strengthen the methodological transparency, clarify results and make the figures more concise and related to the key messages of the paper, and restructure to improve the interpretation and integration of findings within the broader Antarctic climate variability research.

Answer: Thank you for the clear suggestion, we have referred, and cited in relevant sections of the manuscript.

2.3 Climate data and analysis

The $\delta^{18}O$ ($\delta^{18}O$ is preferred because it is highly correlated with δD; r = 0.99), *d*-excess, and SA from the GV7-C ice core were used in the correlation analysis. Two time periods (1957–2013 CE and 1872–2013 CE) were selected for correlation analyses between GV7-C records and climate variables based on data availability (e.g., SAM indices) and to ensure adequate sample size. The annual means of the ice core records derived from multiple intra-annual samples (3–21 data points per year; average 8) were used in the correlation analysis, which reduces the influence of seasonal extreme values. Because isotopic composition recorded in an annual layer reflects integrated snowfall through the year, GV7-C records represent the combined influence of seasonal processes. For the climate data, we therefore examined at both annual (January–December) and seasonal (DJF, MAM, JJA, SON) scales to assess potential relationships. Although some seasonal differences were observed, overall patterns and physical interpretations were consistent when annual means were used; therefore, annual values are presented to represent the net integrated climate signal preserved in the ice core. Correlation analyses were conducted on original and linearly detrended time series (annual and three-year running averages) of the ice core and climate data, and the results are described in Sections 3.3.1 – 3.3.2. The correlation analysis on the smoothed time series were conducted to reduce stratigraphic noise, and at least three-year averaging has been suggested for obtaining a significant climatic signal from the GV7 site (e.g., Frezzotti et al., 2007; Khan et al., 2021; Schlosser and Oerter, 2002). Pearson correlation coefficients were calculated and their significance was assessed using a two-tailed Student's t-test with corresponding *p*-values. Although, the ice core and climate data were annually averaged and linear trends were removed, the effect of autocorrelation on the correlation analysis were tested using effective number of degrees of freedom (N_{eff}) (at $p < 0.01$) (Bretherton et al., 1999). The results indicated negligible autocorrelation effects on the reported correlations (for the correlation coefficients in Tables 4 and 6), and thus the correlations can be considered statistically robust.

For the 1957–2013 CE period, the following climate indices were compared with the annual means of the GV7-C ice core records: station-based SAM index (Marshall G and National Center for Atmospheric Research Staff, 2018), the Southern Oscillation Index (SOI) (https://www.ncei.noaa.gov/access/monitoring/enso/soi), Niño3.4 index (https://psl.noaa.gov/gcoswgsp/Timeseries/Nino34), Indian Ocean Dipole (IOD) index representing the SST gradient between the western and southeastern equatorial IO (https://psl.noaa.gov/gcos_wgsp/Timeseries/DMI), SST anomaly in the southeastern IO (SST-SEIO) (https://psl.noaa.gov/gcos_wgsp/Timeseries/DMI), and reconstructed sea ice extent (SIE) over the Ross–Amundsen Sea sector (162°E–250°E) and the East Antarctic sector (71°E–162°E) (Fogt et al., 2023). Moreover, for the 1957–2013 CE period, spatial correlation analyses (at 95% confidence interval) were conducted between annual GV7-C records and gridded ERA5 reanalysis data (air temperature, SST, sea ice concentration [SIC], 10-m wind speed, zonal [u] and meridional [v] wind components, and total precipitable water) using Climate Reanalyzer developed by the University of Maine, USA (https://climatereanalyzer.org/). Since ice-core isotopic signals reflect a broad range of thermodynamic and dynamic influences, spatial correlation analyses were conducted for physically plausible scenarios to help identify potential moisture supply regions over a longer time period (1957–2013 CE) than previous studies (Caiazzo et al., 2017; Khan, 2019). Spatially coherent and physically interpretable patterns are selectively presented and used as supportive evidence in the interpretation of climate-related signals from the GV7-C ice core. Principal component analysis (PCA), a linear dimensionality reduction technique, was employed to investigate potential similarities in variability between the annual means of the ice-core records and seasonal and annual means of climate datasets (IOD, SST-SEIO, SAM, SOI, Niño3.4, SIE) for 1957–2013 CE. The PCA results conducted on annual mean values were selected and presented in this study. For the 1872–2013 CE period, the GV7-C ice core data were compared with the IOD index, SST-SEIO, reconstructed SST anomaly over the Southern Hemisphere (https://www.ncei.noaa.gov/access/monitoring/climate-at-a-glance/global/time-series) (Huang et al., 2017), reconstructed SAM index (https://psl.noaa.gov/data/20thC_Rean/timeseries/monthly/SAM), and Niño3.4. SAM and ENSO are considered key modes potentially affecting Antarctic climate variability (Turner et al., 2009; Cohen et al., 2012; Pohl et al., 2021; Wille et al., 2021), and the SOI and Niño3.4 indices describe Pacific variability that can influence the climate of the Southern Ocean and Antarctica (Meyerson et al., 2002; Bertler et al., 2004). Moreover, the temperature anomalies (IOD index, SST-SEIO) over the Indian Ocean affects the air temperature (Zhang and Duan, 2023), sea ice extent (Kim et al., 2023; Zhang et al., 2024) and precipitation in Antarctica (Lee et al., 2024).

3.4 Discussion and implications

The variations in SA data from the GV7-C ice core showed significant interannual variations, and show only a weak correlation with IOD and SST-SEIO. The SA of the GV7-C ice core is assumed to be affected by the coupled influence of dynamic processes (i.e., the transport pathways and transport efficiency of moist air) or abrupt synoptic events (e.g., intense transport by atmospheric river events) (Turner et al., 2019; Wille et al., 2021). The variability in SA is affected by moisture transport via large-scale atmospheric circulation (Thomas et al., 2008; Udy et al., 2021; Cohen et al., 2012) and synoptic-scale short-lived events (e.g., atmospheric river events, atmospheric rivers) (Turner et al., 2019; Wille et al., 2021) and evident in the ice core records from coastal regions (Servettaz et al., 2020; Jackson et al., 2023). Moreover, the intensity and frequency of cyclone events also affect snowfall in Antarctic coastal areas (Dalaiden et al., 2020a). Particularly, in the Ross Sea region, the cyclonically driven SA is dominant and the region is sensitive to tropical and local climate drivers (Bertler et al., 2018). The contribution of synoptic-scale transport has been reported to be large for Victoria Land based on simulations over the 1985–2014 period (Dalaiden et al., 2020a). The influence of the ENSO on SA was evident at the Law Dome site (Roberts et al., 2015).

REPLY TO THE COMMENTS BY REVIEWER #2

Dear editor,

The manuscript by Nyamgerel et al. presents a thoughtful investigation of the d18O, dexcess and snow accumulation records preserved in GV7-C ice core layers. Using correlation analyses, they assess how the variability of the GV7-C records may be influenced by climate indices and parameters (e.g., ENSO, SAM, IOD, SST). This manuscript is interesting and relevant and should be considered for publication in Earth System Dynamics. However, some key points need to be reassessed before acceptance for publication in Earth System Dynamics.

Answer: We sincerely thank reviewer #2 for the positive and encouraging assessment of our manuscript. We have carefully considered the comments and revised the manuscript accordingly. Please kindly see the detailed responses provided below

Major comments:

- My main concern is the data treatment prior to applying Pearson's linear correlation. Figure 2 illustrates the annual values for $\delta^{18}O$, δD, and d-excess. Among the mean annual values shown in the figure, some values appear to significantly exceed the mean plus or minus two standard deviations. Despite these notably higher or lower values, the manuscript does not mention an outlier assessment. Additionally, the manuscript fails to address the assessment of data distribution and the potential need for linearization of the records. Furthermore, there is no discussion on whether detrending of datasets is necessary before applying the Pearson's linear correlation. All these steps are crucial, as they could substantially influence the results obtained from Pearson's linear correlation. This is particularly relevant since the main findings of the manuscript depend on the results derived from this correlation. Incorporating these steps into the data treatment would enhance the manuscript.

Answer: We thank for the comment that helped us to improve the materials and method section. We agree that appropriate data preprocessing is essential, since the interpretations rely on correlation analyses.

- Outlier consideration: The annual values shown in Figure 2 may visually appear to exceed ±2 standard deviations in some years. However, these values represent genuine interannual climatic variability rather than analytical artifacts. Each annual mean is derived from multiple intra-annual samples (3–21 data points per year; average 8;), which reduces the influence of seasonal extremes. We retained notable annual values to preserve the continuous climatic signal recorded in the ice core. Removing extreme years may suppress meaningful variability. Therefore, we gently note that no data points were excluded from the correlation analysis.

- Data distribution and linearization, detrending: The analyses are conducted on annual means of the ice core and climate data. Annual averaging reduces the influence of seasonal extreme values.

For the ice core records, depending on the resolution of the records (3–21 data points per year), we were not able obtain continuous seasonal values. For the climate data, we tested/examined at both annual and seasonal (DJF, MAM, JJA, SON) scales to assess potential relationships. Overall patterns and physical interpretations were consistent when annual means were used; therefore, annual values of the climate data were used in the correlation analysis.

We have considered detrending on the time series, in the correlation analyses, we conducted on the original and linearly detrended (removed linear trends to compare the fluctuations in the ice core and climate data) time series of the ice core and climate data, and the results are described in Sections 3.3.1 – 3.3.2. We have also conducted the correlation analysis on annual and three-year running averages. The correlation analysis on the smoothed time series (three-year running averages) were conducted to reduce stratigraphic noise, and at least three-year averaging also has been suggested for obtaining a significant climatic signal from the GV7 site (e.g., Frezzotti et al., 2007; Khan et al., 2021; Schlosser and Oerter, 2002). Pearson correlation coefficients were calculated and their significance was assessed using a two-tailed Student's t-test with corresponding *p*-values.

We also considered the effect of autocorrelation, although, the ice core and climate data were annually averaged and linear trends were removed. The effects of autocorrelation on the correlation analysis were tested using effective number of degrees of freedom (N_{eff}) (at $p < 0.05$) (Bretherton et al., 1999). The results indicated negligible autocorrelation effects on the reported correlations (for the correlation coefficients in Tables 4 and 6), and thus the correlations can be considered statistically robust. We have added the results (Neff ≈ N, indicating negligible autocorrelation effects with p values) for each correlation coefficients, and mentioned the autocorrelation effects in the materials and method section of the revised manuscript.

Table 4. Pearson's correlation coefficients (r) between the GV7-C ice core records and the climate variables for the period 1957–2013 CE. Correlations are calculated for annual data and three-year running averages in the detrended and original time series (shown in parentheses). Larger values ($r > 0.3$ at $p < 0.05$) are marked in bold. SIE (EA) and SIE (RA) denotes sea ice extent over East Antarctica and the Ross-Amundsen Sea sector.

	IOD	SST (SEIO)	SAM	SOI	Niño3.4	SIE (EA)	SIE (RA)
Annual average							
SA	**0.37** (0.28) Neff ≈ N, indicating negligible autocorrelation effects, at p < 0.001	–0.22 (–0.26)	0.12 (0.04)	–0.00 (–0.01)	0.04 (0.04)	0.01 (–0.02)	0.09 (0.00)

$\delta^{18}O$	–0.01 (–0.03)	–0.06 (–0.07)	–0.18 (–0.18)	–0.26 (-0.26)	0.22 (0.22)	–0.06 (–0.07)	–0.23 (–0.22)
d-excess	–0.19 (–0.07)	0.25 **(0.33)**	–0.03 (0.09)	0.02 (0.03)	0.04 (0.05)	–0.05 (0.02)	0.11 (0.22)
Three-year running average							
SA	**0.39** (0.18) Neff ≈ N, indicating negligible autocorrelation effects, at p < 0.0001	**–0.30 (–0.36)** Neff ≈ N, indicating negligible autocorrelation effects, at p < 0.05	0.11 (–0.06)	0.09 (0.09)	–0.11 (–0.14)	0.11 (0.04)	–0.18 (–0.02)
$\delta^{18}O$	–0.06 (–0.02)	0.02 (0.04)	**–0.41** (–0.27) Neff ≈ N, indicating negligible autocorrelation effects, at p < 0.0017	**–0.49 (–0.49)** Neff ≈ N, indicating negligible autocorrelation effects, at p < 0.0001	**0.46 (0.46)** Neff ≈ N, indicating negligible autocorrelation effects, at p < 0.0004	–0.14 (–0.11)	**–0.47 (–0.32)** Neff ≈ N, indicating negligible autocorrelation effects, at p < 0.0002
d-excess	**–0.45** (–0.06) Neff ≈ N, indicating negligible autocorrelation effects, at p < 0.0005	**0.64 (0.72)** Neff ≈ N, indicating negligible autocorrelation effects, at p < 0.0001	–0.15 (–0.21)	–0.11 (–0.09)	0.24 (0.27)	**–0.35** (–0.16) Neff ≈ N, indicating negligible autocorrelation effects, at p < 0.0092	0.01 (0.31)

Table 6. Pearson's correlation coefficients (r) between the GV7-C ice core records and the climate variables for the period 1872–2013 CE. Correlations are calculated for annual data and three-year running averages in the detrended and original time series (shown in parentheses). Larger values ($r > 0.3$ at $p < 0.05$) are marked in underlined bold.

	IOD	SST (SEIO)	SST anomaly	SAM	Niño3.4
Annual average					
SA	0.10 (0.10)	–0.15 (–0.11)	–0.03 (–0.01)	0.03 (0.03)	0.02 (0.02)
$\delta^{18}O$	–0.04 (–0.04)	–0.01 (–0.02)	–0.10 (–0.08)	–0.16 (–0.14)	0.14 (0.13)
d-excess	–0.02 (0.08)	0.02 (0.28)	–0.20 (0.28)	0.06 (0.18)	0.12 (0.13)
Three-year running average					
SA	–0.04 (0.01)	–0.02 (0.02)	–0.04 (0.02)	0.00 (0.04)	0.02 (0.03)
$\delta^{18}O$	–0.12 (–0.11)	0.00 (–0.02)	–0.13 (–0.11)	–0.23 (–0.16)	0.19 (0.18)
d-excess	0.03 (0.23)	**0.32 (0.43)** Neff ≈ N, indicating negligible autocorrelation effects, at p < 0.00017	0.26 **(0.39)**	–0.02 (0.24)	0.24 (0.26)

We have excluded the correlation results on 5-year running averaged as well as 3- and 5-year (point) averages in the revised version, which we considered as unnecessary details. We have revised Section 2.3 as shown below.

"2.3 Climate data and analysis

The $\delta^{18}O$ ($\delta^{18}O$ is preferred because it is highly correlated with δD; r = 0.99), d-excess, and SA from the GV7-C ice core were used in the correlation analysis. Two time periods (1957–2013 CE and 1872–2013 CE) were selected for correlation analyses between GV7-C records and climate variables based on data availability (e.g., SAM indices) and to ensure adequate sample size. The annual means of the ice core records derived from multiple intra-annual samples (3–21 data points per year; average 8) were used in the correlation analysis, which reduces the influence of seasonal extreme values. Because isotopic composition recorded in an annual layer reflects integrated snowfall through the year, GV7-C records represent the combined influence of seasonal processes. For the climate data, we therefore examined at both annual (January–December) and seasonal (DJF, MAM, JJA, SON) scales to assess potential relationships. Although some seasonal differences were observed, overall patterns and physical interpretations were consistent when annual means were used; therefore, annual values are presented to represent the net integrated climate signal preserved in the ice core. Correlation analyses were conducted on original and linearly detrended time series (annual and three-year running averages) of the ice core and climate data, and the results are described in Sections 3.3.1 – 3.3.2. The correlation analysis on the smoothed time series were conducted to reduce stratigraphic noise, and at least three-year averaging has been suggested for obtaining a significant climatic signal from the GV7 site (e.g., Frezzotti et al., 2007; Khan et al., 2021; Schlosser and Oerter, 2002). Pearson correlation coefficients were calculated and their significance was assessed using a two-tailed Student's t-test with corresponding p-values. Although, the ice core and climate data were annually averaged and linear trends were removed, the effect of autocorrelation on the correlation analysis were tested using effective number of degrees of freedom (N_{eff}) (at $p < 0.05$) (Bretherton et al., 1999). The results indicated negligible autocorrelation effects on the reported correlations (for the correlation coefficients in Tables 4 and 6), and thus the correlations can be considered statistically robust."

- The results section presents correlation analyses between annual GV7-C records and annual/seasonal climate variables. Section 2.1 states that snow accumulation at the GV7-C site is higher during austral summer and autumn. This increased snow accumulation during these seasons will inevitably bias the GV7-C annual records ($\delta^{18}O$ and SA) and will consequently affect the results derived from correlating GV7-C annual records with ERA5 annual/seasonal climate variables. Failing to account for this seasonal bias in GV7-C records could lead to misleading interpretations of the relationship between these records and climate variables. Therefore, incorporating a seasonal bias assessment for GV7-C records and discussing this bias will improve the manuscript.

Answer: Thank you for the helpful comment, and we agree on the importance of considering seasonality of the ice core signals. In this study, the age of each sample depth was determined by interpolation between two consecutive $\delta^{18}O$ peaks, with an average of eight data points per year (ranging from 3 to 21). Consequently, some years did not contain sufficient data to represent all seasons or to construct reliable/continuous seasonal records

for $\delta^{18}O$, d-excess, and SA. Therefore, annual values from the GV7-C record were used in this study.

- Section 2.2 indicates that "Annual layers were determined based on the seasonal summer maximum $\delta^{18}O$ peaks in the GV7-C ice core." While there is an explanation of how annual layers were identified, the manuscript lacks information on how the annual averages, which are used to generate most of the results, were calculated. Calculating annual averages from values between summer peaks will capture annual minima during austral winter but may disrupt the continuous representation of annual maxima during austral summer. This is particularly important because annual averages will reflect "better" the "continuous" season and introduce uncertainties regarding the representation of the "discontinuous" season. This approach can lead to some seasons being more prominently represented within the annual average, potentially skewing the correlations. Please provide additional information on how the annual averages were calculated and address the potential effects of divided seasons in both the results analysis and discussion.

Answer: Thank you for the comment regarding potential seasonal bias and the calculation of annual averages. The GV7-C age scale is based on consecutive summer $\delta^{18}O$ maxima, and annual layers are defined accordingly. We note that annual mean values were computed as the mean of all samples assigned to each annual layer (i.e., between two successive summer maxima). As it mentioned in the previous answer, because sampling resolution varies (3–21 samples per year; average 8), some years did not contain sufficient data to represent all seasons or to construct reliable/continuous seasonal records of isotopes. Therefore, annual values from the GV7-C record were used in this study. We also considered that annual averaging would reduce stratigraphic noises.

We have mentioned it in the 2.2. Ice core data section, as it shown below.

2.2 Ice core data

The 78 m long GV7-C ice core was collected in 107 runs and has an average diameter of ~0.08 m. Density was estimated from the mass and dimensions of subsections. Core sections were kept frozen and transported to Korea. In the cold room at the Korea Polar Research Institute (KOPRI), the core was cut to an average sample length of 0.04 m (range 0.03–0.07 m) for stable water isotope analysis ($\delta^{18}O$ and δD). A total of 1880 samples were analyzed using cavity ring-down spectrometers (L2130-I and L2140-i, Picarro Inc., USA) at KOPRI. Annual layers were identified from the seasonal summer maximum $\delta^{18}O$ peaks, and sample ages were assigned by linear interpolation between two consecutive peaks. The GV7-C ice-core record covers 1782–2013 CE. The seasonal $\delta^{18}O$ pattern has been reported previously (Caiazzo et al., 2017; Nardin et al., 2021). Annual layer counting was further constrained using electrical conductivity measurements with a Portable ECM unit (Icefield Instruments Inc., Canada). Conductivity peaks associated with Pinatubo (1991 CE), Agung (1963 CE), Tarawera (1886 CE), Krakatau (1883 CE), and Tambora (1815 CE) were used as additional time markers. Annual mean $\delta^{18}O$, δD, and *d*-excess were calculated as the arithmetic mean of all isotope measurements assigned to each annual layer (i.e., between two successive summer maxima). The annual mean snow accumulation (SA) rate was estimated by multiplying the annual-layer thickness by the measured density of the corresponding core sections and is reported in millimeters water equivalent per year (mm w.e. yr^{-1}). The *d*-excess (*d*-excess = $\delta D - 8 \times \delta^{18}O$) was calculated from $\delta^{18}O$ and δD. Data points per year ranged from 3 to 21 (average 8); some years therefore do not fully resolve all seasons and seasonal means are not consistently available. Accordingly, annual means of $\delta^{18}O$, *d*-excess, and SA are used in the correlation analyses.

- Section 3.2.1 lacks clarity in presenting the data. For instance, lines 188-190 do not explicitly state whether the authors are discussing the 10-m v wind or the 850 hPa v-wind. There also seems to be an inconsistency in reporting the positive or negative correlations between the Pacific Ocean (PO) and Indian Ocean (IO). Similarly, lines 193-194 mention positive correlations between annual d-excess and 2 m/850 hPa temperatures over the western PO and IO sectors. Figure S4 shows positive correlations between annual d-excess and 850 hPa temperatures over the IO sector, but there is no evidence supporting a positive correlation over the western PO sector. It would be very beneficial to include further information about the coverage of the PO and IO sectors, either in Figure 1 or within the text. Section 3.2.1 is complex and difficult to read, and the supporting plots do not provide complete information. For example, Figure S5 presents only the d-excess-SST spatial correlations for DJF and SON. Why are only these presented? Including the entire dataset (annual, DJF, MAM, JJA, and SON) would allow readers to understand how these spatial relationships change throughout the year. The same recommendation applies to all spatial correlations presented. Please reassess the clarity and organization of this section, as it is challenging to follow.

(from minor comment) Line 177: The correlations mentioned in this line cannot be directly traced to the figures in supporting evidence, making it difficult to evaluate the magnitude and spatial distribution of the correlations mentioned in the text. Please, provide figures for the correlations mentioned in the text or remove these statements from the text if the correlations are not relevant.

(from minor comment) Table 5: The table intends to summarise the observed correlations, however, it remains unclear the criteria that has to be met for a correlation to be included in the table and the table is not precise on the magnitude or sign of the correlation. Please, clarify.

Answer: Thank you for the comments related to the spatial correlation analysis.

We revised (mentioned the pairs in the correlation analysis, reorganized, and described in more concise/definite way) the whole section, as shown below.

3.2.2. Spatial correlation analysis with ERA5 reanalysis

Spatial correlation analyses (95% confidence interval) were conducted between annual GV7-C records (δ18O, d-excess, and SA) and annual/seasonal ERA5 reanalysis fields for 1957–2013 CE to explore potential spatial patterns consistent with moisture supply and transport pathways. Significant and physically interpretable patterns are selectively presented in the Supplement (Figs. S1–S3) and are used as supporting evidence in the discussion of likely source regions. For interpretation, the Pacific Ocean (PO) sector is defined here as the western Pacific (90–160°E), Ross Sea (160°E–130°W), and Amundsen–Bellingshausen Seas (130–60°W), while the Indian Ocean (IO) sector is defined as 20–90°E. Annual mean δ18O shows positive correlations with 2 m air temperature and SST primarily over the PO sector (Fig. S1a, b). Positive relationships with air temperature (2 m and 850 hPa) and total column precipitable water are most evident during DJF over parts of the PO and IO sectors (Fig. S1d–f). Negative correlations are observed with sea ice concentration (SIC) over the Ross Sea region (Fig. S1c). Wind-speed correlations (10 m; annual and MAM) are generally negative (Fig. S1g, j), and zonal wind

(u-wind) correlations highlight the belt of strong westerlies (Fig. S1h, k). The meridional wind (v-wind) correlations suggest a northward flow signature from the western PO sector and a southward flow signature from the IO sector during DJF (Fig. S1i), whereas these patterns weaken in MAM (Fig. S1l). Overall, δ18O exhibits its clearest spatial coherence during DJF and MAM, consistent with the seasonality of transport and snowfall in this coastal sector (Delmotte et al., 2000; Caiazzo et al., 2017). These patterns provide qualitative support for a relatively stronger PO-sector influence on δ18O at GV7-C during DJF–MAM, although the overall relationships remain modest.

Annual mean d-excess exhibits positive correlations with air temperature (2 m and 850 hPa) over both the western PO and IO sectors (Fig. S2a–c). Temperature correlations in the IO sector are particularly evident in SON (Fig. S2c), whereas the d-excess response to temperature appears weaker in DJF (not shown). Correlations with SST (SON), SIC (JJA), and total column precipitable water (annual) further support a contribution of air masses from the IO sector and western PO to the GV7 region (Fig. S2d–f). In contrast to δ18O, correlations with wind speed and wind direction are relatively weak, except for a positive correlation with 10 m wind speed in some regions (Fig. S2g). The v-wind pattern indicates a southward flow signature from the IO sector and a northward flow signature in the western PO sector (Fig. S2i). Taken together, these spatial patterns suggest that thermodynamic source-region variability (e.g., SST/air-temperature conditions) may play a comparatively larger role for d-excess at GV7-C than do purely dynamical indicators, and they are consistent with a potentially important contribution from the IO sector, particularly during SON.

No clear and temporally consistent relationships are observed between SA and the investigated climate variables; only weak and spatially limited patterns are identified (Fig. S3). For example, SA shows weak negative correlations with 2 m temperature over parts of the Amundsen Sea coast and weak positive correlations with total column precipitable water offshore of the Ross Sea coast (Fig. S3a, b). SA also shows weak negative correlations with SIC over the Ross Sea region (Fig. S3c). Wind-speed correlations (10 m and 850 hPa) are weakly positive over parts of the PO sector (Fig. S3d, g), and the associated u- and v-wind patterns suggest modest transport signals (Fig. S3e, f, h, i). Overall, these results indicate that SA at GV7-C is likely influenced by multiple factors, including synoptic variability and transport efficiency, which may mask simple relationships with large-scale indices at annual resolution.

In sum, the spatial correlation patterns suggest that GV7-C records reflect regional variability linked to both the PO and IO sectors. The δ18O correlations that are most evident during DJF and MAM motivate consideration of SAM-related dynamical influences during these seasons, while d-excess more strongly reflects thermodynamic variability linked to the IO sector, particularly during SON (Masson-Delmotte et al., 2003).

Moreover, the supplementary spatial-correlation results were consolidated and are now presented as three combined figures (Figs. S1–S3), focusing on the key, physically interpretable patterns that support our discussion.

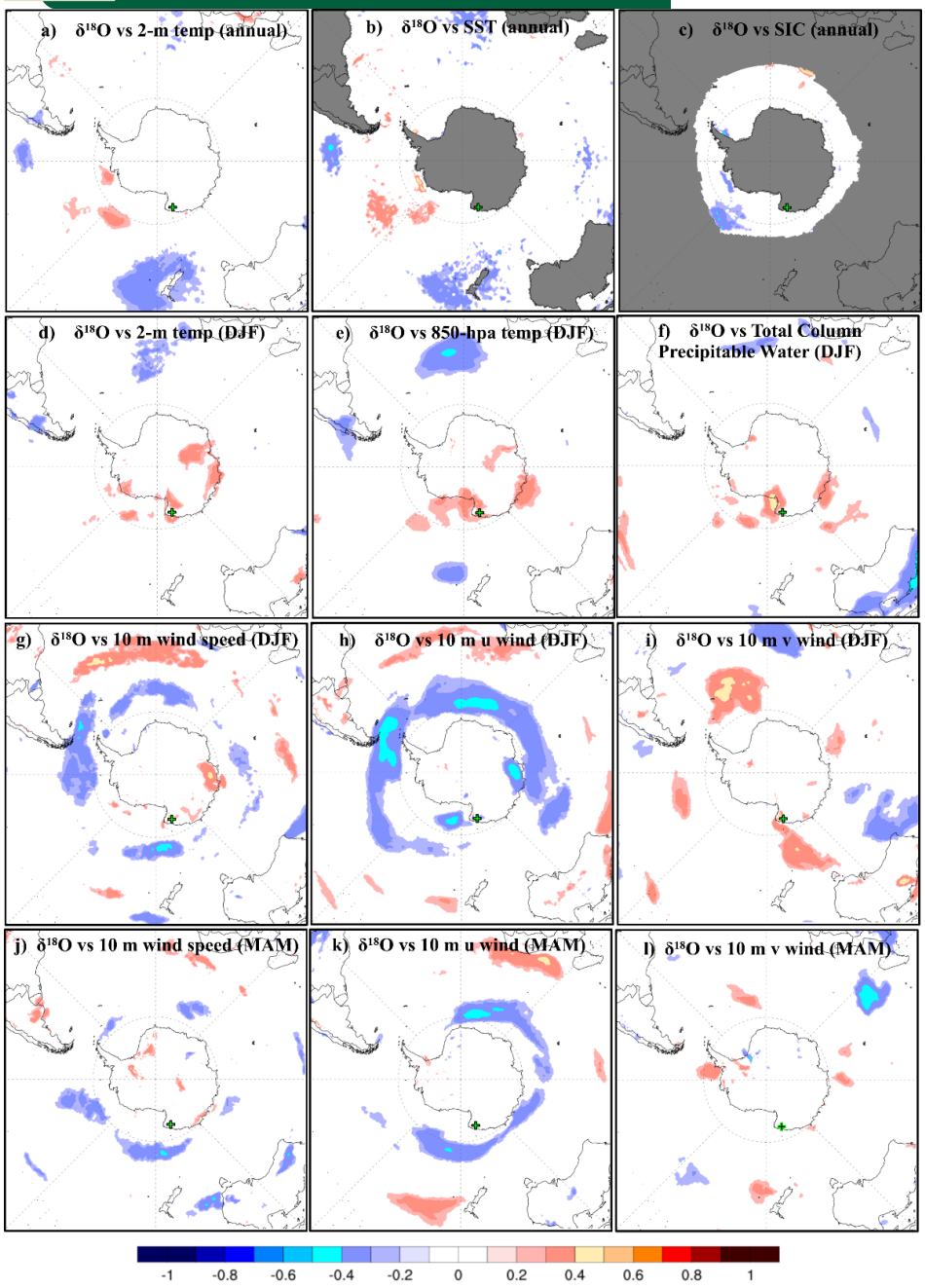


Figure S1. *Spatial correlation of $\delta^{18}O$ with (a, d, e) air temperature, (b) SST, and (c) SIC, (f) total column precipitable water, (g, j) wind speed, (h, k) u-wind components, and (i, l) v-wind components from the ERA5 reanalysis data for different seasons over the 1957–2013 CE period. The scale bars indicate Pearson's correlation coefficient (r) at $p < 0.05$. This figure was generated using Climate Reanalyzer (https://climatereanalyzer.org/) from the Climate Change Institute, University of Maine, USA.*

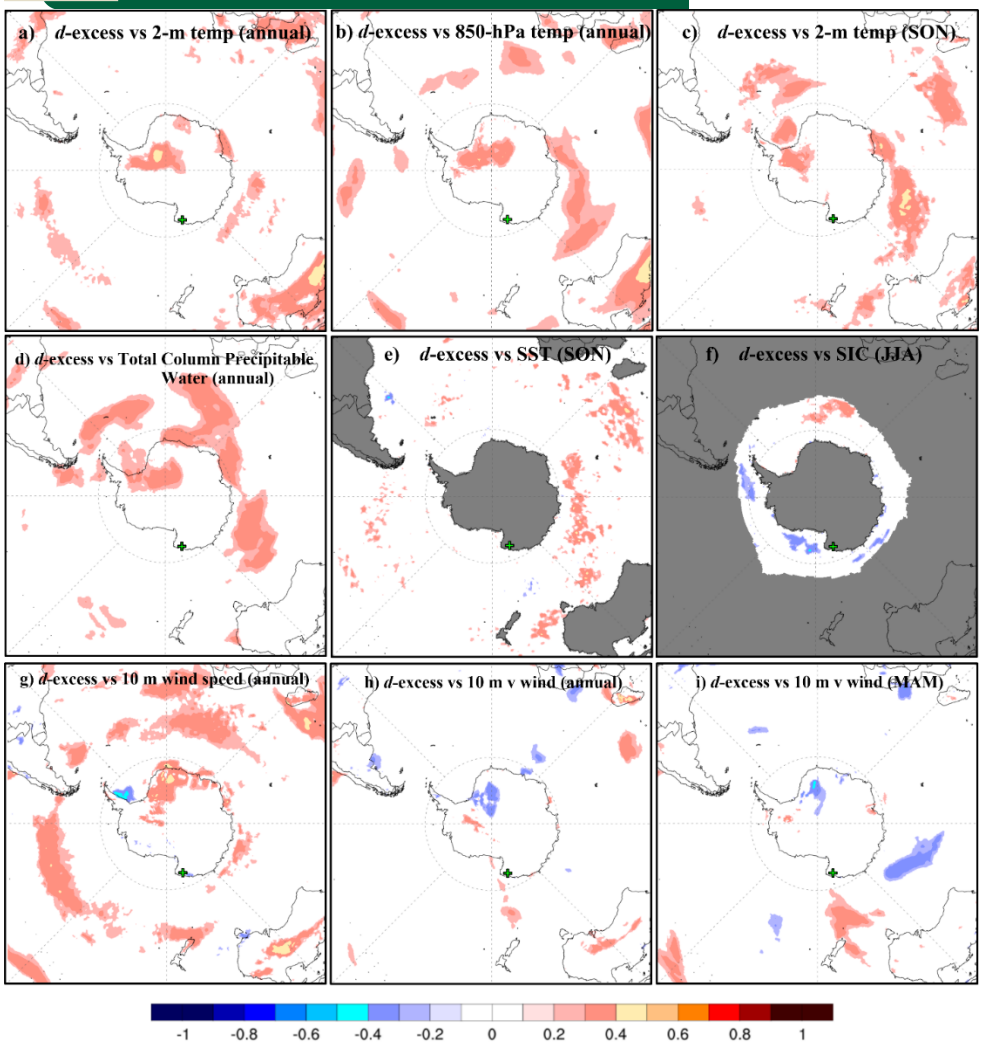


Figure S1. *Spatial correlation of d-excess with the (a, b, c) air temperature, (d) total column precipitable water, (e) SST, (f) SIC, (g) 10 m wind speed and (h, i) v-wind component from ERA5 reanalysis data for different seasons over the 1957–2013 CE period. The scale bars indicate Pearson's correlation coefficient (r) at $p < 0.05$. This figure was generated using Climate Reanalyzer (https://climatereanalyzer.org/) from the Climate Change Institute, University of Maine, USA.*

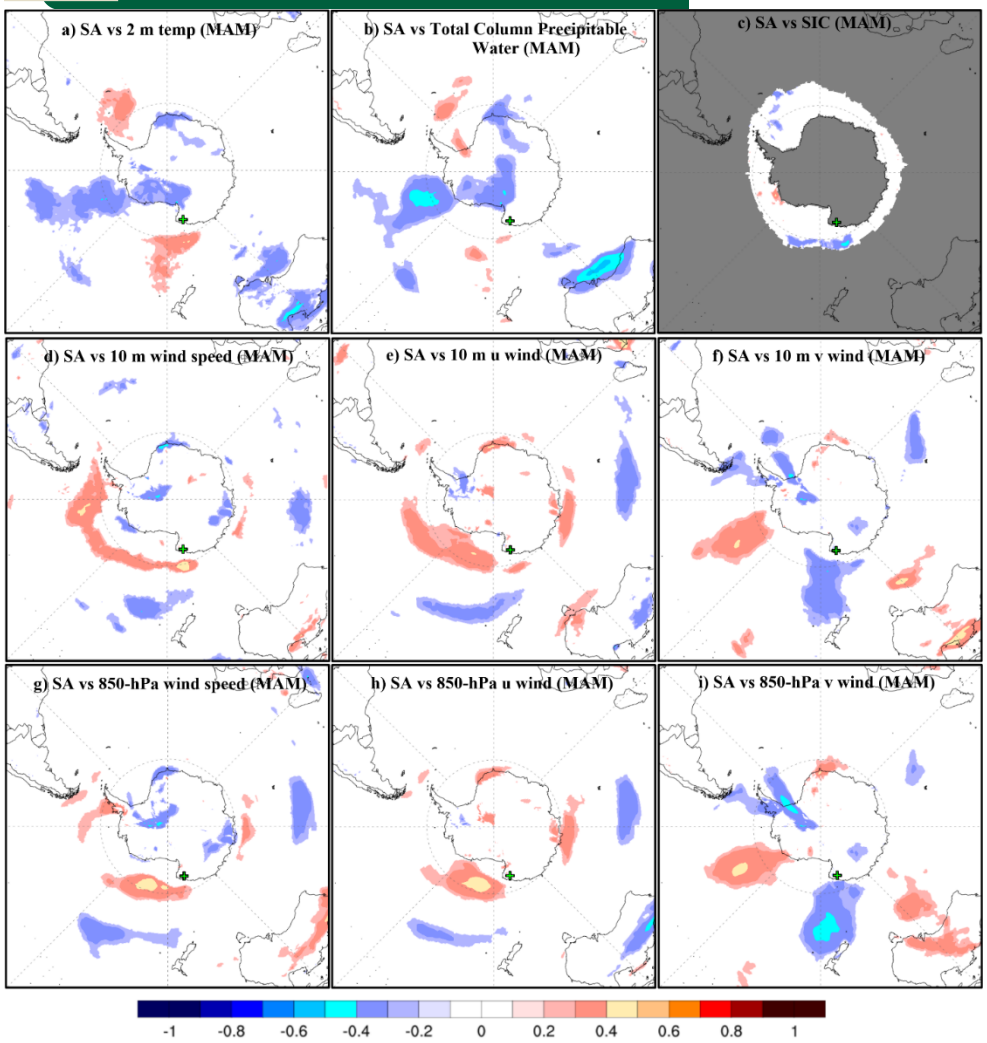


Figure S3. *Spatial correlation of SA with (a) air temperature, (b) total column precipitable water, (c) SIC, (d, g) 10 m wind speed, (e, h) u-wind components, and (f, i) v-wind components from ERA5 reanalysis data during the MAM season over the 1957–2013 CE period. The scale bars indicate Pearson's correlation coefficient (r) at $p < 0.05$. This figure was generated using Climate Reanalyzer (https://climatereanalyzer.org/) from the Climate Change Institute, University of Maine, USA.*

- Section 3.2.2 is quite challenging to read due to the amount of information presented without a clear structure. I recommend that the authors review the organization of this section, focusing on clearly conveying the main information relevant to supporting their arguments.

Answer: Thank you for the comment. We reorganized and streamlined this section to improve readability, removed duplications and unnecessary details, and clarified which spatial-correlation results are central to supporting our interpretations.

The edited section is shown below.

3.3.2 Climate Signals for the Long-Term Records (1872–2013 CE)

The GV7-C ice core data were also compared with long-term records (1872–2013 CE) for the SAM, Niño3.4, IOD, SST-SEIO, and SST anomaly over the Southern Hemisphere (Fig. 4 and Table 6). Pearson's correlation coefficients (r) between the GV7-C ice core records and the climate variables are shown in Table 4. Correlations are calculated for annual and three-year running averages in detrended time series. Correlations on original time series were also shown as comparison to the detrended results, and the results were comparable (Table 6). For the $\delta^{18}O$ and SA, no significant correlations were found with the climate variables in this period. This disappearance suggesting the smoothing of signal intensity due to various influencing factors. Considering the correlation of $\delta^{18}O$ with Niño3.4 ($r = 0.46$) and SOI ($r = -0.49$) for 1957–2013 CE (Table 4), this suggests the influence of SST changes in the PO sector. However, this correlation weakened over a longer period (1872–2013). However, some evident relevance can still be observed in the short-term period for $\delta^{18}O$ and SA. The decrease in SA during the 1876–1885 CE and 1940–1955 CE periods was consistent with the increasing trend in the SAM. The recent trend (1985–2013) for $\delta^{18}O$ was also found to be in line with Niño3.4 and the SAM index (Fig. 4). While the *d*-excess was correlated with SST-SEIO ($r = 0.32$, $n = 140$, $p < 0.001$) in the three-year averaged time series. (Table 6 and Fig. 4). The spatial correlation of *d*-excess with the reconstructed SST dataset was also tested for two periods: 1957–2013 CE, and 1854–2013 CE (Fig. 5). Weak positive correlations were observed over the remote IO sector during the 1957–2013 CE period (Fig. 5a) while in the period from 1854 to 2013 CE, the correlation was observed over a larger area in the southern sector of the IO (Fig. 5b). Therefore, the *d*-excess signal from the GV7-C ice core can be roughly suggested to representing thermodynamic changes (i.e., SST changes) over the IO sector of the Southern Ocean, at least over the 1872–2013 CE period.

As we mentioned in the previous comment, we have excluded the correlation results on 5-year running averaged as well as 3- and 5-year (point) averages in the revised version (for 1957–2013 as well as 1872–2013), which we considered as unnecessary details. Corresponding tables and figures are changes as shown below.

Table 4. Pearson's correlation coefficients (r) between the GV7-C ice core records and the climate variables for the period 1957–2013 CE. Correlations are calculated for annual data and three-year running averages in the detrended and original time series (shown in parentheses). Larger values ($r > 0.3$ at $p < 0.05$) are marked in bold. SIE (EA) and SIE (RA) denotes sea ice extent over East Antarctica and the Ross-Amundsen Sea sector.

	IOD	SST (SEIO)	SAM	SOI	Niño3.4	SIE (EA)	SIE (RA)
Annual average							
SA	**0.37** (0.28)	–0.22 (–0.26)	0.12 (0.04)	–0.00 (–0.01)	0.04 (0.04)	0.01 (–0.02)	0.09 (0.00)
$\delta^{18}O$	–0.01 (–0.03)	–0.06 (–0.07)	–0.18 (–0.18)	–0.26 (-0.26)	0.22 (0.22)	–0.06 (–0.07)	–0.23 (–0.22)

d-excess	–0.19 (–0.07)	0.25 **(0.33)**	–0.03 (0.09)	0.02 (0.03)	0.04 (0.05)	–0.05 (0.02)	0.11 (0.22)
Three-year running average							
SA	**0.39** (0.18)	**–0.30 (–0.36)**	0.11 (–0.06)	0.09 (0.09)	–0.11 (–0.14)	0.11 (0.04)	–0.18 (–0.02)
$\delta^{18}O$	–0.06 (–0.02)	0.02 (0.04)	**–0.41** (–0.27)	**–0.49 (–0.49)**	**0.46 (0.46)**	–0.14 (–0.11)	**–0.47 (–0.32)**
d-excess	**–0.45** (–0.06)	**0.64 (0.72)**	–0.15 (–0.21)	–0.11 (–0.09)	0.24 (0.27)	**–0.35** (–0.16)	0.01 (0.31)

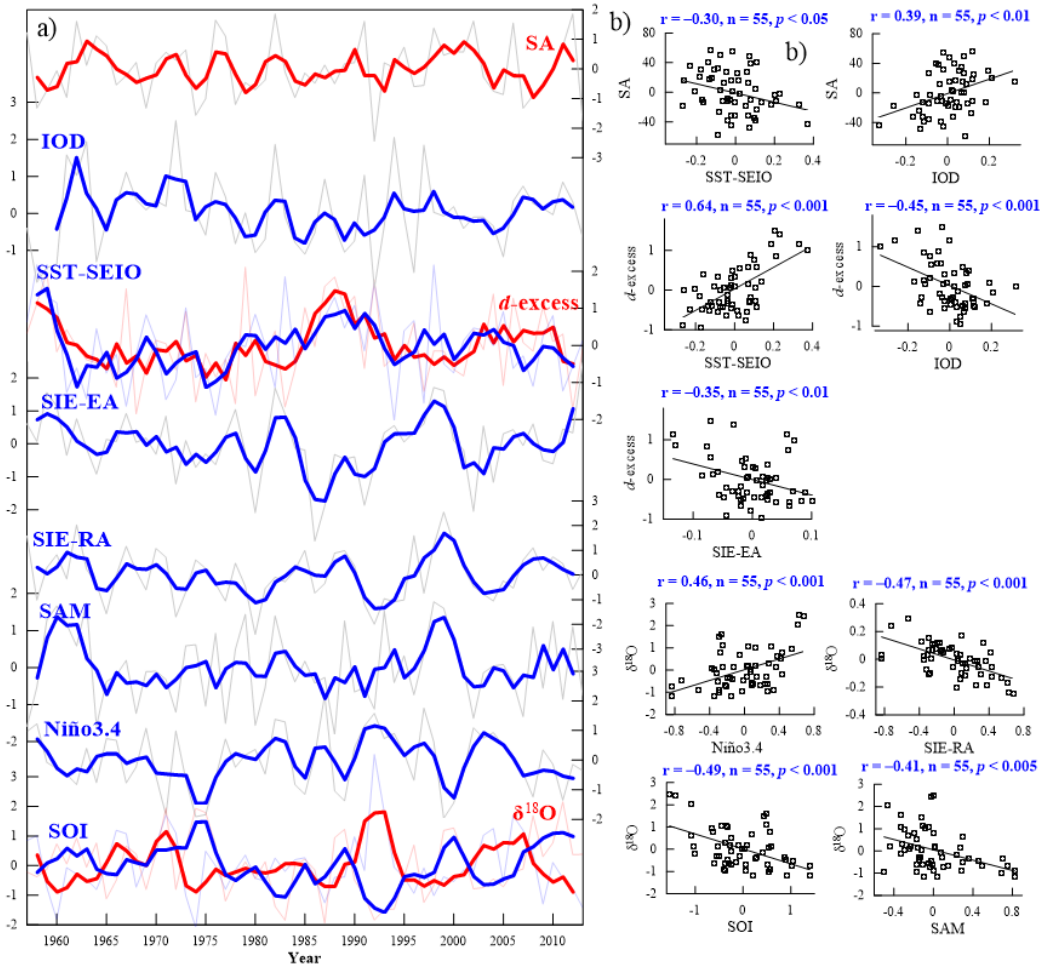


Figure 3. Comparison of the standardized profiles (grey lines) for detrended time series of SA, $\delta^{18}O$, and *d*-excess with the climate variables for 1957–2013 CE (a). The thick lines (blue and red) indicate the 3-year running average. Linear regression profiles for the 3-year running averaged time series are also shown with significant correlation coefficients (at $p < 0.05$) (b).

Minor comments:

Line 25: Please consider specifying…large variations in the "near surface" air temperature….

Answer: Thank you for the helpful comment, we have edited accordingly.

1 Introduction

Climate variability over Antarctica and the surrounding Southern Ocean is crucial for the global climate system (Mayewski et al., 2009; Fretwell et al., 2013; Rintoul et al., 2018). However, the Antarctic climate system is complex (Masson-Delmotte et al., 2008), with large variations in near-surface air temperature (Nicolas and Bromwich, 2014; Constable et al., 2022) and surface mass balance (Dalaiden et al., 2020a), sparse observational coverage, and high natural variability (Kim et al., 2020; Klein et al., 2019), with particularly pronounced variability in coastal regions (Tuohy et al., 2015; Stenni et al., 2017; Goursaud et al., 2019). Ice-core records provide a means to reconstruct past climatic and environmental conditions. Stable water isotopes

Line 39: Changes in atmospheric circulation "patterns"

Answer: Thank you for the helpful comment, we have edited accordingly.

1 Introduction

Climate variability over Antarctica and the surrounding Southern Ocean is crucial for the global climate system (Mayewski et al., 2009; Fretwell et al., 2013; Rintoul et al., 2018). However, the Antarctic climate system is complex (Masson-Delmotte et al., 2008), with large variations in near-surface air temperature (Nicolas and Bromwich, 2014; Constable et al., 2022) and surface mass balance (Dalaiden et al., 2020a), sparse observational coverage, and high natural variability (Kim et al., 2020; Klein et al., 2019), with particularly pronounced variability in coastal regions (Tuohy et al., 2015; Stenni et al., 2017; Goursaud et al., 2019). Ice-core records provide a means to reconstruct past climatic and environmental conditions. Stable water isotopes ($\delta^{18}O$ and δD) in ice cores can reflect relative changes in temperature (Jouzel et al., 1997; Markle and Steig, 2022), sea ice extent (SIE), and atmospheric circulation (Thomas and Abram, 2016). Atmospheric circulation patterns have been reported as important factors influencing isotopic signals in Antarctic ice cores (Bertler et al., 2004; Kino et al., 2021; Leroy-Dos Santos et al., 2023). The relationships between isotopes, temperature, and surface mass balance depend on the relative contributions of large-scale dynamical and thermodynamic processes (Oerter et al., 2000; Medley et al., 2018; Goursaud et al., 2019; Dalaiden et al., 2020b). Moreover, the influence of the Southern Annular Mode (SAM), which describes shifts in the Southern

Lines 44-46: This sentence is not clear: "In recent decades, the Southern Annular Mode (SAM), which indicates the modulation of westerly winds towards the Southern Hemisphere (Hall and Visbeck, 2002; Fogt et al., 2012), has become increasingly important for the Southern Hemisphere climate (Russell and McGregor, 2010).". Does this mean that before the recent decades, SAM had no major relevance in the Southern Hemisphere climate? Please specify.

Answer: Thank you for the comment. We revised and reorganized the Introduction for clarity and to avoid wording that could imply that SAM was irrelevant prior to recent decades.

1 Introduction

Climate variability over Antarctica and the surrounding Southern Ocean is crucial for the global climate system (Mayewski et al., 2009; Fretwell et al., 2013; Rintoul et al., 2018). However, the Antarctic climate system is complex (Masson-Delmotte et al., 2008), with large variations in near-surface air temperature (Nicolas and Bromwich, 2014; Constable et al., 2022) and surface mass balance (Dalaiden et al., 2020a), sparse observational coverage, and high natural variability (Kim et al., 2020; Klein et al., 2019), with particularly pronounced variability in coastal regions (Tuohy et al., 2015; Stenni et al., 2017; Goursaud et al., 2019). Ice-core records provide a means to reconstruct past climatic and environmental conditions. Stable water isotopes ($\delta^{18}O$ and δD) in ice cores can reflect relative changes in temperature (Jouzel et al., 1997; Markle and Steig, 2022), sea ice extent (SIE), and atmospheric circulation (Thomas and Abram, 2016). Atmospheric circulation patterns have been reported as important factors influencing isotopic signals in Antarctic ice cores (Bertler et al., 2004; Kino et al., 2021; Leroy-Dos Santos et al., 2023). The relationships between isotopes, temperature, and surface mass balance depend on the relative contributions of large-scale dynamical and thermodynamic processes (Qerter et al., 2000; Medley et al., 2018; Goursaud et al., 2019; Dalaiden et al., 2020b). Moreover, the influence of the Southern Annular Mode (SAM), which describes shifts in the Southern Hemisphere westerlies (Hall and Visbeck, 2002; Fogt et al., 2012), has been evidenced in $\delta^{18}O$ and surface mass balance records from coastal Antarctic ice cores (Schlosser et al., 2014; Servettaz et al., 2020). The second-order parameter *d*-excess (*d*-excess = $\delta D - 8 \times \delta^{18}O$), which is sensitive to relative humidity and sea-surface temperature (SST) at the moisture source (Jouzel et al., 1982; Delmotte et al., 2000; Uemura et al., 2008), has been used to infer source-region conditions (Stenni et al., 2001; Sodemann and Stohl, 2009). Snow accumulation (SA) rates estimated from ice cores can also respond to changes in moisture availability and circulation, and may increase in warmer climates (Frieler et al., 2015; Palerme et al., 2017) and under low sea-ice conditions in coastal regions (Nyamgerel et al., 2020), although the strength and mechanisms of these relationships can be site dependent (Dalaiden et al., 2020a).

In recent decades, SAM variability has exerted a strong influence on Southern Hemisphere climate (Russell and McGregor, 2010), affecting the spatial variability of temperature, precipitation, and sea ice across Antarctica (Nicolas and Bromwich, 2014; Purich et al., 2016; Kim et al., 2020). Antarctic surface mass balance is also linked to the El Niño–Southern Oscillation (ENSO) (Kim et al., 2020). Teleconnections between Antarctic and tropical climate variability have been reported in ice-core

Line 60: It is mentioned that the study aims to explore the climate-related signals in the GV7-C ice core record (including dD). However, the dD signal is not explored in depth (only included in the manuscript through the d-excess). Please include the dD record on the analyses or remove dD from the list of the records that will be explored in the study.

Answer: Thank you for the helpful comment, we mentioned about it in the following section.

2.3 Climate data and analysis

The $\delta^{18}O$ ($\delta^{18}O$ is preferred because it is highly correlated with δD; r = 0.99), *d*-excess, and SA from the GV7-C ice core were used in the correlation analysis. Two time periods (1957–2013 CE and 1872–2013 CE) were selected for correlation analyses between GV7-C records and climate variables based on data availability (e.g., SAM indices) and to ensure adequate
105 sample size. The annual means of the ice core records derived from multiple intra-annual samples (3–21 data points per year; average 8) were used in the correlation analysis, which reduces the influence of seasonal extreme values. Because isotopic composition recorded in an annual layer reflects integrated snowfall through the year, GV7-C records represent the combined influence of seasonal processes. For the climate data, we therefore examined at both annual (January–December) and seasonal (DJF, MAM, JJA, SON) scales to assess potential relationships. Although some seasonal differences were

Line 72: it is mentioned that the site is 95km away from the coastline, however, the coastline is “permanently” covered with perennial sea ice (as seen in Fig 1). It would be useful to know how far is the site from the open water. Please add this info.

Answer: Thank you for the helpful comment. As you mentioned, depending on the perennial sea ice, the distance to open water (not the coastline) would be differed. We kept this mentioning the distance to coastline “of the Southern Ocean”, as it shown below.

2 Materials and methods

2.1 Study area

During the 2013/14 Antarctic summer season, a collaborative Italian/Korean expedition drilled several firn-ice cores at the GV7 drilling site (70°41′ S, 158°52′ E; 1950 m a.s.l.), located on the Oates Coast of East Antarctic (Fig. 1). Six shallow firn cores (ranging from 5 and 50 m in length) and intermediate firn-ice cores (ranging from 78 and 250 m in length) were drilled. The 78m deep core, named GV7-C, is used and presented in this study. The site is approximately 95 km away from the nearest coastline of the Southern Ocean, and the ice velocity at this location is very low (< 0.3 m yr^{-1}) (Frezzotti et al., 2007), and the 10-m firn temperature was measured to be –31.8 °C (Frezzotti et al., 2007). Notably, the SA rate in this area is relatively high,

Line 76-80: The information in these lines seem to disagree. The first line says that during autumn-winter airmasses primarily originate from WPO and during spring the from the Ross sector. Then, the next line says airmasses (2007-2012) are from the Indian Ocean and Antarctic Plateau with smaller contributions from the Ross Sea and PO. These sentences don’t say much unless the evaluation time period is specified in the first sentence. Please evaluate clarifying the information in these lines.

Answer: Thank you for the helpful comment, we have edited accordingly.

Frezzotti et al., 2007; Magand et al., 2004). Based on the records from 2007 to 2012, during the autumn–winter period, the air mass primarily originates from the western Pacific Ocean (PO) sector, while the spring period is characterized by dominant input from the Ross Sea sector, with prevailing winds from the south (Caiazzo et al., 2017). Back trajectory estimations revealed that the dominant air mass pathways are from the Indian Ocean (IO) (32%) and the Antarctic Plateau (29%) (Caiazzo et al., 2017), while the Ross Sea and western PO sectors account for 21% and 19%, respectively. Furthermore, the western PO

Line 82-83: Please specify which parameter is the one that exhibits the second maximum in winter. If it is the SA, please specify.

Answer: Thank you for the helpful comment, we have edited accordingly.

and IO sectors accounted for 59% (147 mm) and 28% (69 mm) of the total precipitation (250 mm), respectively (Caiazzo et al., 2017). The SA at this site was estimated to be higher in austral summer and autumn (Caiazzo et al., 2017). Notably, the western PO sector also exhibits a second maximum SA in winter, with the trajectory pathway indicating dominance from the Antarctica Plateau and the IO sector.

Figure1: Please add a reference to the geographical location of the oates coast. Figure 1: Please add elevation contours to the map. Figure 1: There are grey and green dots in the map, please add a legend stating what they mean

Answer: Thank you for your comment, we have edited accordingly. We excluded the lines representing the sea ice extent since it mentioned once only (not discussed further).

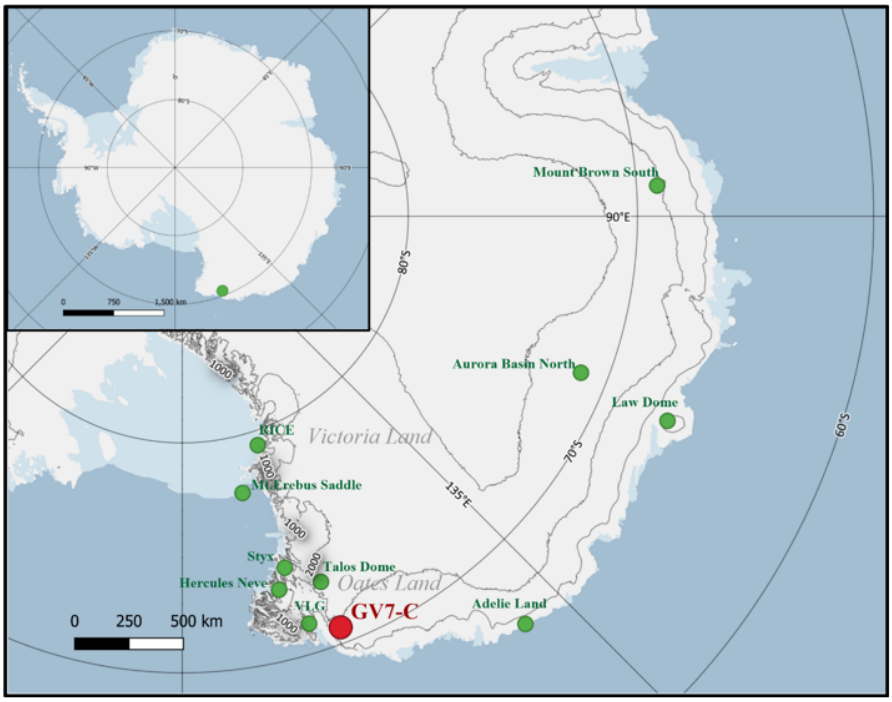


Figure 1. Location of the GV7-C ice core (red) and other ice core sites (green) in East Antarctica. RAMP2 elevation contours (1000 m) are shown (Liu et al., 2015). The map was generated using QGIS software with Quantarctica3 project data (Matsuoka et al., 2021).

Line 98: how was the electrical conductivity measured? Please, specify.

Answer: Thank you for the comment, we have edited accordingly.

2.1 Study area

During the 2013/14 Antarctic summer season, a collaborative Italian/Korean expedition drilled several firn-ice cores at the GV7 drilling site (70°41′ S, 158°52′ E; 1950 m a.s.l.), located on the Oates Coast of East Antarctic (Fig. 1). Six shallow firn cores (ranging from 5 and 50 m in length) and intermediate firn-ice cores (ranging from 78 and 250 m in length) were drilled. The 78m deep core, named GV7-C, is used and presented in this study. The site is approximately 95 km away from the nearest coastline of the Southern Ocean, and the ice velocity at this location is very low (< 0.3 m yr^{-1}) (Frezzotti et al., 2007), and the 10-m firn temperature was measured to be –31.8 °C (Frezzotti et al., 2007). Notably, the SA rate in this area is relatively high, while the post-depositional effect is low due to the low intensity of katabatic winds along the ice divide (Becagli et al., 2004;

Line 99-101: The manuscript doesn't mention about the SA estimation accounting for compression. Please specify why.

Answer: Thank you for the helpful comment, the annual mean SA rate was calculated in water-equivalent units by multiplying the depth corresponding to one full year by the measured density of each section of the ice core. We also note that vertical strain thinning effect would be minimal given the shallow depth (78 m) and relatively short temporal coverage (233 years).

2.2 Ice core data

The 78 m long GV7-C ice core was collected in 107 runs and has an average diameter of ~0.08 m. Density was estimated from the mass and dimensions of subsections. Core sections were kept frozen and transported to Korea. In the cold room at the Korea Polar Research Institute (KOPRI), the core was cut to an average sample length of 0.04 m (range 0.03–0.07 m) for stable water isotope analysis ($\delta^{18}O$ and δD). A total of 1880 samples were analyzed using cavity ring-down spectrometers (L2130-I and L2140-i, Picarro Inc., USA) at KOPRI. Annual layers were identified from the seasonal summer maximum $\delta^{18}O$ peaks, and sample ages were assigned by linear interpolation between two consecutive peaks. The GV7-C ice-core record covers 1782–2013 CE. The seasonal $\delta^{18}O$ pattern has been reported previously (Caiazzo et al., 2017; Nardin et al., 2021). Annual layer counting was further constrained using electrical conductivity measurements with a Portable ECM unit (Icefield Instruments Inc., Canada). Conductivity peaks associated with Pinatubo (1991 CE), Agung (1963 CE), Tarawera (1886 CE), Krakatau (1883 CE), and Tambora (1815 CE) were used as additional time markers. Annual mean $\delta^{18}O$, δD, and *d*-excess were calculated as the arithmetic mean of all isotope measurements assigned to each annual layer (i.e., between two successive summer maxima). The annual mean snow accumulation (SA) rate was estimated by multiplying the annual-layer thickness by the measured density of the corresponding core sections and is reported in millimeters water equivalent per year (mm w.e. yr^{-1}). The *d*-excess (*d*-excess = $\delta D - 8 \times \delta^{18}O$) was calculated from $\delta^{18}O$ and δD. Data points per year ranged from 3 to 21 (average 8); some years therefore do not fully resolve all seasons and seasonal means are not consistently available. Accordingly, annual means of $\delta^{18}O$, *d*-excess, and SA are used in the correlation analyses.

Lines 103-107: Please specify why the evaluation period goes back only to 1957, when ERA5 extends from 1950-present.

Answer: Thank you for the comment. We clarified in the Methods why two evaluation periods are used. The 1957–2013 CE period was selected to maximize overlap among the observational/reconstructed indices used (including SAM) and to ensure a robust and consistent comparison across datasets; the longer 1872–2013 CE period is used where longer climate reconstructions are available.

2.3 Climate data and analysis

The $\delta^{18}O$ ($\delta^{18}O$ is preferred because it is highly correlated with δD; r = 0.99), *d*-excess, and SA from the GV7-C ice core were used in the correlation analysis. Two time periods (1957–2013 CE and 1872–2013 CE) were selected for correlation analyses between GV7-C records and climate variables based on data availability (e.g., SAM indices) and to ensure adequate sample size. The annual means of the ice core records derived from multiple intra-annual samples (3–21 data points per year; average 8) were used in the correlation analysis, which reduces the influence of seasonal extreme values. Because isotopic composition recorded in an annual layer reflects integrated snowfall through the year, GV7-C records represent the combined influence of seasonal processes. For the climate data, we therefore examined at both annual (January–December) and seasonal (DJF, MAM, JJA, SON) scales to assess potential relationships. Although some seasonal differences were observed, overall patterns and physical interpretations were consistent when annual means were used; therefore, annual values are presented to represent the net integrated climate signal preserved in the ice core. Correlation analyses were conducted on original and linearly detrended time series (annual and three-year running averages) of the ice core and climate data, and the results are described in Sections 3.3.1 – 3.3.2. The correlation analysis on the smoothed time series were conducted to reduce stratigraphic noise, and at least three-year averaging has been suggested for obtaining a significant climatic signal from the GV7 site (e.g., Frezzotti et al., 2007; Khan et al., 2021; Schlosser and Oerter, 2002). Pearson correlation coefficients were calculated and their significance was assessed using a two-tailed Student's t-test with corresponding *p*-values. Although, the ice core and climate data were annually averaged and linear trends were removed, the effect of autocorrelation on the correlation analysis were tested using effective number of degrees of freedom (N_{eff}) (at $p < 0.01$) (Bretherton et al., 1999). The results indicated negligible autocorrelation effects on the reported correlations (for the correlation coefficients in Tables 4 and 6), and thus the correlations can be considered statistically robust.

Line 127: The datasets are presented and evaluated in "periods". Please specify in the methods section the reason to evaluate the datasets in these particular time periods.

Answer: Thank you for the helpful comment, we have edited the section 2.3. Climate data and analysis which was unclear about data processing. Two time periods (1957–2013 CE and 1872–2013 CE) were considered, plainly depending on the availability of the climate data (e.g., SAM index) and to ensure a large sample size compared to previous studies in this site. Now the edited parts can be seen as shown in below.

2.3 Climate data and analysis

The $\delta^{18}O$ ($\delta^{18}O$ is preferred because it is highly correlated with δD; r = 0.99), *d*-excess, and SA from the GV7-C ice core were used in the correlation analysis. Two time periods (1957–2013 CE and 1872–2013 CE) were selected for correlation analyses between GV7-C records and climate variables based on data availability (e.g., SAM indices) and to ensure adequate sample size. The annual means of the ice core records derived from multiple intra-annual samples (3–21 data points per year; average 8) were used in the correlation analysis, which reduces the influence of seasonal extreme values. Because isotopic composition recorded in an annual layer reflects integrated snowfall through the year, GV7-C records represent the combined influence of seasonal processes. For the climate data, we therefore examined at both annual (January–December) and seasonal (DJF, MAM, JJA, SON) scales to assess potential relationships. Although some seasonal differences were observed, overall patterns and physical interpretations were consistent when annual means were used; therefore, annual values are presented to represent the net integrated climate signal preserved in the ice core. Correlation analyses were conducted on original and linearly detrended time series (annual and three-year running averages) of the ice core and climate data, and the results are described in Sections 3.3.1 – 3.3.2. The correlation analysis on the smoothed time series were conducted to reduce stratigraphic noise, and at least three-year averaging has been suggested for obtaining a significant climatic signal from the GV7 site (e.g., Frezzotti et al., 2007; Khan et al., 2021; Schlosser and Oerter, 2002). Pearson correlation coefficients were calculated and their significance was assessed using a two-tailed Student's t-test with corresponding *p*-values. Although, the ice core and climate data were annually averaged and linear trends were removed, the effect of autocorrelation on the correlation analysis were tested using effective number of degrees of freedom (N_{eff}) (at $p < 0.01$) (Bretherton et al., 1999). The results indicated negligible autocorrelation effects on the reported correlations (for the correlation coefficients in Tables 4 and 6), and thus the correlations can be considered statistically robust.

For the 1957–2013 CE period, the following climate indices were compared with the annual means of the GV7-C ice core records: station-based SAM index (Marshall G and National Center for Atmospheric Research Staff, 2018), the Southern Oscillation Index (SOI) (https://www.ncei.noaa.gov/access/monitoring/enso/soi), Niño3.4 index (https://psl.noaa.gov/gcoswgsp/Timeseries/Nino34), Indian Ocean Dipole (IOD) index representing the SST gradient between the western and southeastern equatorial IO (https://psl.noaa.gov/gcos_wgsp/Timeseries/DMI), SST anomaly in the southeastern IO (SST-SEIO) (https://psl.noaa.gov/gcos_wgsp/Timeseries/DMI), and reconstructed sea ice extent (SIE) over the Ross–Amundsen Sea sector (162°E–250°E) and the East Antarctic sector (71°E–162°E) (Fogt et al., 2023). Moreover, for the 1957–2013 CE period, spatial correlation analyses (at 95% confidence interval) were conducted between annual GV7-C records and gridded ERA5 reanalysis data (air temperature, SST, sea ice concentration [SIC], 10-m wind speed, zonal [u] and meridional [v] wind components, and total precipitable water) using Climate Reanalyzer developed by the University of Maine, USA (https://climatereanalyzer.org/). Since ice-core isotopic signals reflect a broad range of thermodynamic and dynamic influences, spatial correlation analyses were conducted for physically plausible scenarios to help identify potential moisture supply regions over a longer time period (1957–2013 CE) than previous studies (Caiazzo et al., 2017; Khan, 2019). Spatially coherent and physically interpretable patterns are selectively presented and used as supportive evidence in the interpretation of climate-related signals from the GV7-C ice core. Principal component analysis (PCA), a linear dimensionality reduction technique, was employed to investigate potential similarities in variability between the annual means of the ice-core records and seasonal and annual means of climate datasets (IOD, SST-SEIO, SAM, SOI, Niño3.4, SIE) for 1957–2013 CE. The PCA results conducted on annual mean values were selected and presented in this study. For the 1872–2013 CE period, the GV7-C ice core data were compared with the IOD index, SST-SEIO, reconstructed SST anomaly over the Southern Hemisphere (https://www.ncei.noaa.gov/access/monitoring/climate-at-a-glance/global/time-series) (Huang et al., 2017), reconstructed SAM index (https://psl.noaa.gov/data/20thC_Rean/timeseries/monthly/SAM), and Niño3.4. SAM and ENSO are considered key modes potentially affecting Antarctic climate variability (Turner et al., 2009; Cohen et al., 2012; Pohl et al., 2021; Wille et al., 2021), and the SOI and Niño3.4 indices describe Pacific variability that can influence the climate of the Southern Ocean and Antarctica (Meyerson et al., 2002; Bertler et al., 2004). Moreover, the temperature anomalies (IOD index, SST-SEIO) over the Indian Ocean affects the air temperature (Zhang and Duan, 2023), sea ice extent (Kim et al., 2023; Zhang et al., 2024) and precipitation in Antarctica (Lee et al., 2024).

Line 129: It is mentioned six periods, however, Figure 2 shows seven periods and there are seven periods in between brackets in line 130. Please, correct for consistency.

Answer: Thank you for the comment, we have edited accordingly.

3 Results and discussion

3.1 Characterization of the GV7-C ice core record

The descriptive statistics for the annual mean $\delta^{18}O$, δD, *d*-excess, and SA in the GV7-C ice core are presented in Table 1. The results are also presented in five different time scales at around 50-year intervals (Table 1). Linear regression of $\delta^{18}O$ with δD and *d*-excess were reported for all data and the five different time scales, as well as for annually averaged values, annual maxima, and annual minima (Table 2). For the whole 1782–2013 CE period, the annual mean $\delta^{18}O$ in the GV7-C ice core (n = 233) fluctuated between −32.92‰ and −24.60‰, while δD ranged from −259.42‰ to −210.21‰. The annual variation in $\delta^{18}O$, *d*-excess, and SA is presented in Figure 2, revealing large interannual and decadal-scale variations. Sequential years (at least five) with smaller (or colder) than average $\delta^{18}O$ (−29.64‰) were observed for seven periods (1838–1842 CE, 1858–1862 CE, 1880–1885 CE, 1904–1908 CE, 1918–1922 CE, 1960–1965 CE, and 1995–2002 CE). Additionally, the years between 1977 CE and 1991 CE were lower than average, except for 1979 CE, 1982 CE, 1985 CE, and 1990 CE. In addition, sequential

Line 132: Is mentioned that there are four periods with sequential years higher than the average. However, figure 2 only shows three periods. Please, correct for consistency.

Answer: Thank you for the comment, we have edited accordingly.

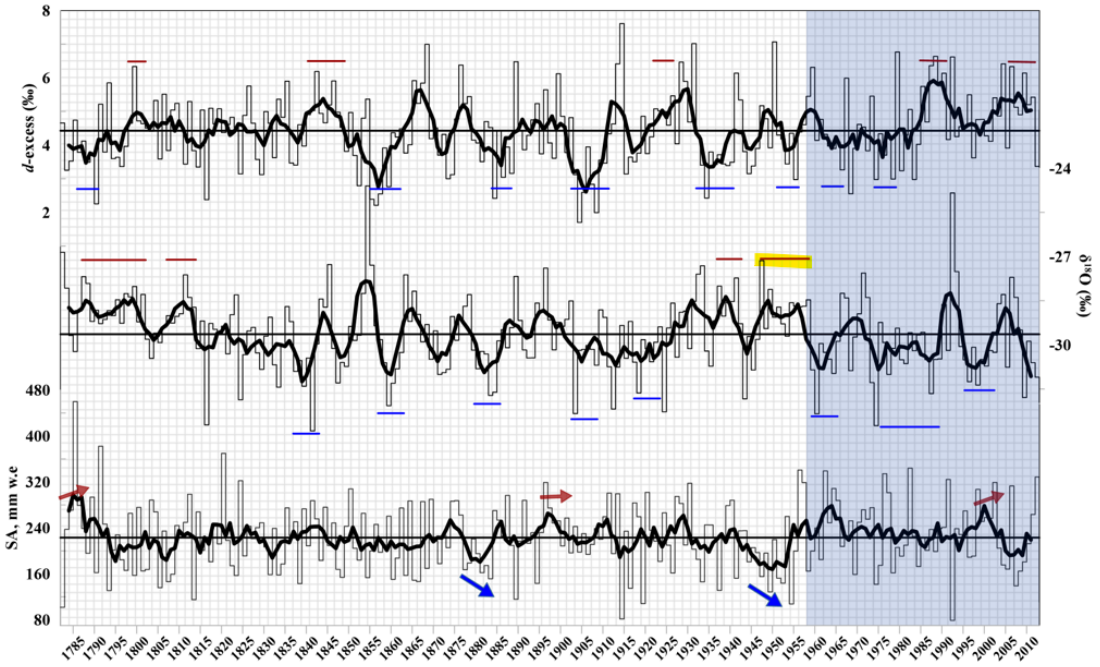


Figure 2. Temporal variation in the SA (bottom panel), $\delta^{18}O$ (middle panel), and *d*-excess (top panel), with the horizontal black line indicating the overall mean. The thick black lines represent the 5-year running average. The blue and red lines (arrows) indicate the periods that are higher or lower than average for at least four continuous years.

Line 132: Periods are reported without a temporal unit (CE), not matching previously reported periods in Line 130.

Answer: Thank you, we have edited accordingly.

3 Results and discussion

3.1 Characterization of the GV7-C ice core record

The descriptive statistics for the annual mean $\delta^{18}O$, δD, *d*-excess, and SA in the GV7-C ice core are presented in Table 1. The results are also presented in five different time scales at around 50-year intervals (Table 1). Linear regression of $\delta^{18}O$ with δD and *d*-excess were reported for all data and the five different time scales, as well as for annually averaged values, annual maxima, and annual minima (Table 2). For the whole 1782–2013 CE period, the annual mean $\delta^{18}O$ in the GV7-C ice core (n = 233) fluctuated between −32.92‰ and −24.60‰, while δD ranged from −259.42‰ to −210.21‰. The annual variation in $\delta^{18}O$, *d*-excess, and SA is presented in Figure 2, revealing large interannual and decadal-scale variations. Sequential years (at least five) with smaller (or colder) than average $\delta^{18}O$ (−29.64‰) were observed for seven periods (1838–1842 CE, 1858–1862 CE, 1880–1885 CE, 1904–1908 CE, 1918–1922 CE, 1960–1965 CE, and 1995–2002 CE). Additionally, the years between 1977 CE and 1991 CE were lower than average, except for 1979 CE, 1982 CE, 1985 CE, and 1990 CE. In addition, sequential years (at least six) higher than the average were observed for 1787–1801 CE, 1807–1813 CE, 1937–1942 CE, and 1948–1958 CE (except 1953) (Fig. 2). The linear relationship between $\delta^{18}O$ and δD ($\delta D = 8.46 \times \delta^{18}O + 17.97$, $R^2 = 0.99$, n = 1880, $p < 0.001$) had a slope slightly larger than that for the precipitation isotopic composition both globally (8) (Craig, 1961) and on the Antarctic–wide scale (7.75) (Masson-Delmotte et al., 2008). The slopes derived for the different time scales ranged from 8.35 (for 1982–2013 CE) to 8.67 (for 1882–1931 CE) (Table 2).

Line 138-139: The manuscript lists eight periods while Figure 2 only highlights seven. Please, correct for consistency.

Answer: Thank you for the helpful comment, we have edited accordingly.

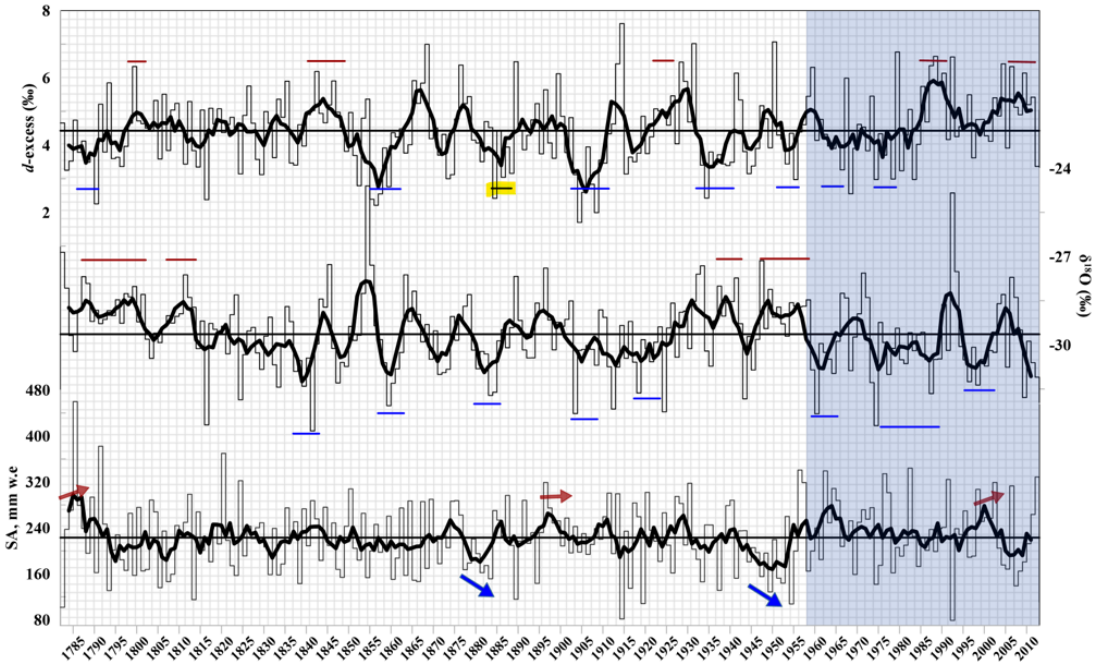


Figure 2. Temporal variation in the SA (bottom panel), $\delta^{18}O$ (middle panel), and *d*-excess (top panel), with the horizontal black line indicating the overall mean. The thick black lines represent the 5-year running average. The blue and red lines (arrows) indicate the periods that are higher or lower than average for at least four continuous years.

Table 1,2 & 3: The evaluation periods have higher "n" values than the annual evaluation. Please specify in the methods section what data is being used when comparing the evaluation "periods"

Answer: Thank you for the helpful comment, we have edited accordingly. Table 2 and 3 are combined in one table and we reorganized as it shown in below. We also mentioned it in 3.1. section.

Table 2. Linear regression analysis for $\delta^{18}O$ with δD and *d*-excess from the GV7-C ice core.

	Slope	Intercept	R^2	*p*-value	n
		$\delta^{18}O$ vs δD			
1782–2013 CE (all data)	8.46	17.97	0.99	<0.0001	1880
1782–1831 CE	8.54	20.12	0.99	<0.0001	344
1832–1881 CE	8.44	17.60	0.99	<0.0001	355
1882–1931 CE	8.67	24.36	0.99	<0.0001	399
1932–1981 CE	8.51	19.41	0.99	<0.0001	429
1982–2013 CE	8.35	15.51	0.99	<0.0001	353
Annual mean	8.17	9.64	0.99	<0.0001	233
Annual maximum	8.27	13.57	0.98	<0.0001	233
Annual minimum	8.19	9.07	0.99	<0.0001	233
		$\delta^{18}O$ vs *d*-excess			
1782–2013 CE (all data)	0.46	18.07	0.21	<0.0001	1880
1782–1831 CE	0.54	20.04	0.24	<0.0001	344
1832–1881 CE	0.45	17.83	0.18	<0.0001	355
1882–1931 CE	0.67	24.33	0.34	<0.0001	399
1932–1981 CE	0.52	19.45	0.24	<0.0001	429
1982–2013 CE	0.36	15.62	0.18	<0.0001	353
Annual mean	0.18	9.68	0.04	<0.0001	233
Annual maximum	0.28	14.45	0.10	<0.0001	233
Annual minimum	0.26	10.68	0.09	<0.0001	233

3 Results and discussion

3.1 Characterization of the GV7-C ice core record

The descriptive statistics for the annual mean $\delta^{18}O$, δD, *d*-excess, and SA in the GV7-C ice core are presented in Table 1. The results are also presented in five different time scales at around 50-year intervals (Table 1). Linear regression of $\delta^{18}O$ with δD and *d*-excess were reported for all data and the five different time scales, as well as for annually averaged values, annual maxima, and annual minima (Table 3). For the whole 1782–2013 CE period, the annual mean $\delta^{18}O$ in the GV7-C ice core (n = 233) fluctuated between –32.92‰ and –24.60‰, while δD ranged from –259.42‰ to –210.21‰. The annual variation in

Line 178-179: the manuscript brings attention to “the correlations”, however, it remains unclear to which correlations the authors are referring (positive? negative?). Please, clarify.

Answer: Thank you for the comment, we have edited accordingly.

“Annual mean $\delta^{18}O$ shows positive correlations with 2 m air temperature and SST primarily over the PO sector (Fig. S1a, b). Positive relationships with air temperature (2 m and 850 hPa) and total column precipitable water are most evident during DJF over parts of the PO and IO sectors (Fig. S1d–f). Negative correlations are observed with sea ice concentration (SIC) over the Ross Sea region (Fig. S1c).”.

Figure 3: Please add values to each vertical axis for reference.”

We edited Figure 3 as shown below.

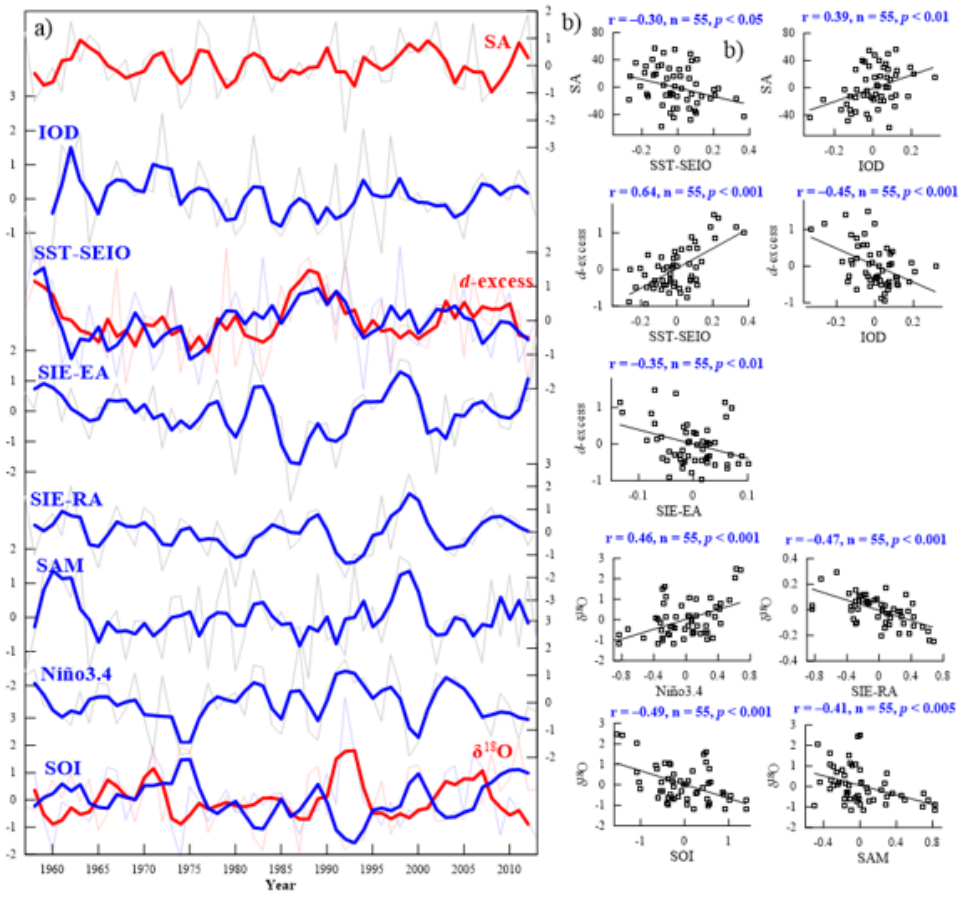


Figure 3. Comparison of the standardized profiles (grey lines) for detrended time series of SA, $\delta^{18}O$, and *d*-excess with the climate variables for 1957–2013 CE (a). The thick lines (blue and red) indicate the 3-year running average. Linear regression profiles for the 3-year running averaged time series are also shown with significant correlation coefficients (at $p < 0.05$) (b).

Line 297: the manuscript states correlations were performed using the running-averaged data. Why not the non-averaged data? Also, it seems that they only used the 5-year running-averaged data. Why not the 3-year running-averaged data? It is not clear from the manuscript why they use some datasets and not all the ones they generated.

Answer: Thank you for the helpful comment, again helped us to reconsider the concise reporting of the results.

We have added results for annual averages (non-averaged) for 1957–2013 and 1872–2013. We also tested the correlation coefficients on the original and linearly detrended (shown in parentheses) time series of the ice core and climate data. We have excluded the correlation results on 5-year running averaged as well as 3- and 5-year (point) averages in the revised version, which we considered as unnecessary details.

We edited the table captions (which was unclear in the previous version).

Table 4. Pearson's correlation coefficients (r) between the GV7-C ice core records and the climate variables for the period 1957–2013 CE. Correlations are calculated for annual data and three-year running averages in the detrended and original time series (shown in parentheses). Larger values ($r > 0.3$ at $p < 0.05$) are marked in bold. SIE (EA) and SIE (RA) denotes sea ice extent over East Antarctica and the Ross-Amundsen Sea sector.

	IOD	SST (SEIO)	SAM	SOI	Niño3.4	SIE (EA)	SIE (RA)
				Annual average			
SA	**0.37** (0.28)	–0.22 (–0.26)	0.12 (0.04)	–0.00 (–0.01)	0.04 (0.04)	0.01 (–0.02)	0.09 (0.00)
$\delta^{18}O$	–0.01 (–0.03)	–0.06 (–0.07)	–0.18 (–0.18)	–0.26 (-0.26)	0.22 (0.22)	–0.06 (–0.07)	–0.23 (–0.22)
d-excess	–0.19 (–0.07)	0.25 **(0.33)**	–0.03 (0.09)	0.02 (0.03)	0.04 (0.05)	–0.05 (0.02)	0.11 (0.22)
				Three-year running average			
SA	**0.39** (0.18)	**–0.30 (–0.36)**	0.11 (–0.06)	0.09 (0.09)	–0.11 (–0.14)	0.11 (0.04)	–0.18 (–0.02)
$\delta^{18}O$	–0.06 (–0.02)	0.02 (0.04)	**–0.41** (–0.27)	**–0.49 (–0.49)**	**0.46 (0.46)**	–0.14 (–0.11)	**–0.47 (–0.32)**
d-excess	**–0.45** (–0.06)	**0.64 (0.72)**	–0.15 (–0.21)	–0.11 (–0.09)	0.24 (0.27)	**–0.35** (–0.16)	0.01 (0.31)

Table 6. Pearson's correlation coefficients (r) between the GV7-C ice core records and the climate variables for the period 1872–2013 CE. Correlations are calculated for annual data and three-year running averages in the detrended and original time series (shown in parentheses). Larger values ($r > 0.3$ at $p < 0.05$) are marked in underlined bold.

	IOD	SST (SEIO)	SST anomaly	SAM	Niño3.4
			Annual average		
SA	0.10 (0.10)	–0.15 (–0.11)	–0.03 (–0.01)	0.03 (0.03)	0.02 (0.02)
$\delta^{18}O$	–0.04 (–0.04)	–0.01 (–0.02)	–0.10 (–0.08)	–0.16 (–0.14)	0.14 (0.13)
d-excess	–0.02 (0.08)	0.02 (0.28)	–0.20 (0.28)	0.06 (0.18)	0.12 (0.13)
			Three-year running average		
SA	–0.04 (0.01)	–0.02 (0.02)	–0.04 (0.02)	0.00 (0.04)	0.02 (0.03)
$\delta^{18}O$	–0.12 (–0.11)	0.00 (–0.02)	–0.13 (–0.11)	–0.23 (–0.16)	0.19 (0.18)
d-excess	0.03 (0.23)	**0.32 (0.43)**	0.26 **(0.39)**	–0.02 (0.24)	0.24 (0.26)

We also edited the result section which was quite wordy and unclear.

3.3 Correlation analysis for 1957–2013 CE and 1872–2013 CE periods

3.3.1 Climate signals for the 1957–2013 CE period

The SAM, Niño3.4, SOI, IOD, SST-SEIO, and SIE data were compared with the $\delta^{18}O$, *d*-excess, SA of the GV7-C ice core. The standardized values of the variables for 1957–2013 CE are presented in Figure 3. The $\delta^{18}O$ exhibited three periods of higher values (1964–1971 CE, 1989–1993 CE, and 2001–2007 CE) (Fig. 3), while the *d*-excess remained generally flat before 1983 and showed two periods of higher values (1985–1992, 2002–2011). The SA values showed significant interannual variations. Pearson's correlation coefficients (r) between the GV7-C ice core records and the climate variables are shown in Table 4. Correlations are calculated for annual and three-year running averages in detrended time series. Correlations on original time series were also shown as comparison to the detrended results, and the results were comparable (Table 4). For the annual mean time series, no significant correlations were found, except that SA show a weak correlation to IOD ($r = 0.37$, $p < 0.05$, $n = 57$). Furthermore, SA kept weak positive correlations with IOD ($r = 0.39$, $p < 0.01$ $n = 55$) and SST-SEIO ($r = -0.30$, $p < 0.05$ $n = 55$) in the three-year running averaged time series. While the $\delta^{18}O$ exhibited correlations with SAM ($r = -0.41$, $p < 0.005$, $n = 55$), SOI ($r = -0.49$, $p < 0.001$, $n = 55$), Niño3.4 ($r = 0.46$, $p < 0.001$, $n = 55$), and SIE over the Ross-Amundsen Sea ($r = -0.47$, $p < 0.001$, $n = 55$) in the three-year running-averaged time series. For *d*-excess, there was a moderate correlation with SST-SEIO ($r = 0.64$, $p < 0.001$ $n = 55$), and weak correlations with the IOD ($r = -0.45$, $p < 0.001$, $n = 55$), and SIE over the East Antarctic sector ($r = -0.35$, $p < 0.001$, $n = 55$). Overall, the correlation analysis likely to suggest the variations in the $\delta^{18}O$ (for the 1957–2013 CE) capture the climatic signals over the tropical PO as well as the southern sector of the PO, indicating the contribution of air mass originating from this region. While the *d*-excess likely to indicates the climatic signals (sea surface temperature) over the southeastern IO, and this relevance indicate the air mass intrusion from this region. Moreover, the climatic conditions over the Indian Ocean sector appear to have reflected in the SA of the ice core.

PCA analysis conducted for 1957–2013 CE, with the loading matrix (correlation coefficients at $p < 0.05$) presented in Table 5. Principal component (PC) 1 clustered $\delta^{18}O$, the SAM, SOI, Niño3.4, and SIE over the East Antarctica and Ross-Amundsen Sea region. This reflected the importance of both thermodynamic and dynamic effects on the decrease (increase) in $\delta^{18}O$ with an increase (decrease) in the SIE, stronger (weaker) westerly winds (i.e., the SAM and SOI), and lower (higher) SSTs in the Niño3.4 region. In PC 2, *d*-excess and SA were clustered with IOD, SAM, SIE, and particularly strong signal of SST-SEIO. This can represent the increasing (decreasing) *d*-excess with increased (decreased) evaporation with warm (cold) SSTs particularly over the southeastern IO. Moreover, there could be a weak relevance with enhanced (weakened) air mass transport with strong westerlies (i.e., the SAM), consequent wind-induced increase (decrease) in SIE over East Antarctica and relatively cooler temperature over the eastern IO (decreasing IOD). It is ambiguous to explain the negative correlation between the SA and SST-SEIO in PC 2. However, PC 3 included SA only, with more stronger signals of IOD, SAM, SOI, Niño3.4 and SIE over the East Antarctica. This can represent the thermodynamic effects on SA with increased (decreased) evaporation with warm SSTs over western equatorial IO and central tropical PO (i.e., the SOI and Niño3.4), enhanced moisture transport with strong westerlies (i.e., the SAM), and the wind-induced SIE over East Antarctica. PC 4 was characterized by an increasing (decreasing) $\delta^{18}O$, *d*-excess with decreasing (increasing) SST-SEIO which can be explained by the intrusion of different air masses with evident *d*-excess signals together with $\delta^{18}O$. Overall, PCA classified the variables into species representing the climatic signals corresponding to the PO (PC 1) and southeastern IO sector of the Southern Ocean (PC 2). Interestingly, the relatively strong detectability of the thermodynamic effect on *d*-excess, which is induced by the IO sector, likely to indicate the significant (detectable) temperature signals in this region.

3.3.2 Climate Signals for the Long-Term Records (1872–2013 CE)

The GV7-C ice core data were also compared with long-term records (1872–2013 CE) for the SAM, Niño3.4, IOD, SST-SEIO, and SST anomaly over the Southern Hemisphere (Fig. 4 and Table 6). Pearson's correlation coefficients (r) between the GV7-C ice core records and the climate variables are shown in Table 4. Correlations are calculated for annual and three-year running averages in detrended time series. Correlations on original time series were also shown as comparison to the detrended results, and the results were comparable (Table 6). For the $\delta^{18}O$ and SA, no significant correlations were found with the climate variables in this period. This disappearance suggesting the smoothing of signal intensity due to various influencing factors. Considering the correlation of $\delta^{18}O$ with Niño3.4 ($r = 0.46$) and SOI ($r = -0.49$) for 1957–2013 CE (Table 4), this suggests the influence of SST changes in the PO sector. However, this correlation weakened over a longer period (1872–2013). However, some evident relevance can still be observed in the short-term period for $\delta^{18}O$ and SA. The decrease in SA during the 1876–1885 CE and 1940–1955 CE periods was consistent with the increasing trend in the SAM. The recent trend (1985–2013) for $\delta^{18}O$ was also found to be in line with Niño3.4 and the SAM index (Fig. 4). While the *d*-excess was correlated with SST-SEIO ($r = 0.32$, $n = 140$, $p < 0.001$) in the three-year averaged time series. (Table 6 and Fig. 4). The spatial correlation of *d*-excess with the reconstructed SST dataset was also tested for two periods: 1957–2013 CE, and 1854–2013 CE (Fig. 5). Weak positive correlations were observed over the remote IO sector during the 1957–2013 CE period (Fig. 5a) while in the period from 1854 to 2013 CE, the correlation was observed over a larger area in the southern sector of the IO (Fig. 5b). Therefore, the *d*-excess signal from the GV7-C ice core can be roughly suggested to representing thermodynamic changes (i.e., SST changes) over the IO sector of the Southern Ocean, at least over the 1872–2013 CE period.

Lines 312-324: it is not clear if the authors are reporting results obtained using the 3-year or 5-year running-averaged data. Please specify.

Answer: Thank you for the comment. We revised the Results section to explicitly state when 3-year versus 5-year running means are used and to make the presentation of smoothed versus unsmoothed results clearer.

3.3.2 Climate Signals for the Long-Term Records (1872–2013 CE)

The GV7-C ice core data were also compared with long-term records (1872–2013 CE) for the SAM, Niño3.4, IOD, SST-SEIO, and SST anomaly over the Southern Hemisphere (Fig. 4 and Table 6). Pearson's correlation coefficients (r) between the GV7-C ice core records and the climate variables are shown in Table 4. Correlations are calculated for annual and three-year running averages in detrended time series. Correlations on original time series were also shown as comparison to the detrended results, and the results were comparable (Table 6). For the $\delta^{18}O$ and SA, no significant correlations were found with the climate variables in this period. This disappearance suggesting the smoothing of signal intensity due to various influencing factors. Considering the correlation of $\delta^{18}O$ with Niño3.4 ($r = 0.46$) and SOI ($r = -0.49$) for 1957–2013 CE (Table 4), this suggests the influence of SST changes in the PO sector. However, this correlation weakened over a longer period (1872–2013). However, some evident relevance can still be observed in the short-term period for $\delta^{18}O$ and SA. The decrease in SA during the 1876–1885 CE and 1940–1955 CE periods was consistent with the increasing trend in the SAM. The recent trend (1985–2013) for $\delta^{18}O$ was also found to be in line with Niño3.4 and the SAM index (Fig. 4). While the *d*-excess was correlated with SST-SEIO ($r = 0.32$, $n = 140$, $p < 0.001$) in the three-year averaged time series. (Table 6 and Fig. 4). The spatial correlation of *d*-excess with the reconstructed SST dataset was also tested for two periods: 1957–2013 CE, and 1854–2013 CE (Fig. 5). Weak positive correlations were observed over the remote IO sector during the 1957–2013 CE period (Fig. 5a) while in the period from 1854 to 2013 CE, the correlation was observed over a larger area in the southern sector of the IO (Fig. 5b). Therefore, the *d*-excess signal from the GV7-C ice core can be roughly suggested to representing thermodynamic changes (i.e., SST changes) over the IO sector of the Southern Ocean, at least over the 1872–2013 CE period.

Table 8: I find very difficult to understand this table. What does the number inside the parenthesis mean? The caption says "Pearson's correlation coeficcients between three- and

five-year average (in parenthesis) and…". According to what is written in the caption, I understand that what it is in parenthesis is the five-year average correlation coefficient. However, the last four rows of the table are exclusively dedicated to presenting the data for the 5-year running-average dataset and it also has numbers in parenthesis. Please consider adding information in the table caption about how to interpret table 8.

Answer: Thank you for the helpful comment, we have edited the table captions (which was unclear in the previous version).

We edited the table captions (which was unclear in the previous version).

Table 4. Pearson's correlation coefficients (r) between the GV7-C ice core records and the climate variables for the period 1957–2013 CE. Correlations are calculated for annual data and three-year running averages in the detrended and original time series (shown in parentheses). Larger values ($r > 0.3$ at $p < 0.05$) are marked in bold. SIE (EA) and SIE (RA) denotes sea ice extent over East Antarctica and the Ross-Amundsen Sea sector.

	IOD	SST (SEIO)	SAM	SOI	Niño3.4	SIE (EA)	SIE (RA)
				Annual average			
SA	**0.37** (0.28)	–0.22 (–0.26)	0.12 (0.04)	–0.00 (–0.01)	0.04 (0.04)	0.01 (–0.02)	0.09 (0.00)
$\delta^{18}O$	–0.01 (–0.03)	–0.06 (–0.07)	–0.18 (–0.18)	–0.26 (-0.26)	0.22 (0.22)	–0.06 (–0.07)	–0.23 (–0.22)
d-excess	–0.19 (–0.07)	0.25 **(0.33)**	–0.03 (0.09)	0.02 (0.03)	0.04 (0.05)	–0.05 (0.02)	0.11 (0.22)
				Three-year running average			
SA	**0.39** (0.18)	**–0.30 (–0.36)**	0.11 (–0.06)	0.09 (0.09)	–0.11 (–0.14)	0.11 (0.04)	–0.18 (–0.02)
$\delta^{18}O$	–0.06 (–0.02)	0.02 (0.04)	**–0.41** (–0.27)	**–0.49 (–0.49)**	**0.46 (0.46)**	–0.14 (–0.11)	**–0.47 (–0.32)**
d-excess	**–0.45** (–0.06)	**0.64 (0.72)**	–0.15 (–0.21)	–0.11 (–0.09)	0.24 (0.27)	**–0.35** (–0.16)	0.01 (0.31)

Table 6. Pearson's correlation coefficients (r) between the GV7-C ice core records and the climate variables for the period 1872–2013 CE. Correlations are calculated for annual data and three-year running averages in the detrended and original time series (shown in parentheses). Larger values ($r > 0.3$ at $p < 0.05$) are marked in underlined bold.

	IOD	SST (SEIO)	SST anomaly	SAM	Niño3.4
			Annual average		
SA	0.10 (0.10)	–0.15 (–0.11)	–0.03 (–0.01)	0.03 (0.03)	0.02 (0.02)
$\delta^{18}O$	–0.04 (–0.04)	–0.01 (–0.02)	–0.10 (–0.08)	–0.16 (–0.14)	0.14 (0.13)
d-excess	–0.02 (0.08)	0.02 (0.28)	–0.20 (0.28)	0.06 (0.18)	0.12 (0.13)
			Three-year running average		
SA	–0.04 (0.01)	–0.02 (0.02)	–0.04 (0.02)	0.00 (0.04)	0.02 (0.03)
$\delta^{18}O$	–0.12 (–0.11)	0.00 (–0.02)	–0.13 (–0.11)	–0.23 (–0.16)	0.19 (0.18)
d-excess	0.03 (0.23)	**0.32 (0.43)**	0.26 **(0.39)**	–0.02 (0.24)	0.24 (0.26)

Line 347: Please consider adding the word “partly” to “…(decreasing) d18O can be _____ explained by the intrusion…”.

Answer: Thank you for the comment, we have edited accordingly.

3.4 Discussion and implications

The variations in SA data from the GV7-C ice core showed significant interannual variations, and show only a weak correlation with IOD and SST-SEIO. The SA of the GV7-C ice core is assumed to be affected by the coupled influence of dynamic processes (i.e., the transport pathways and transport efficiency of moist air) or abrupt synoptic events (e.g., intense transport by atmospheric river events) (Turner et al., 2019; Wille et al., 2021). The variability in SA is affected by moisture transport via large-scale atmospheric circulation (Thomas et al., 2008; Udy et al., 2021; Cohen et al., 2012) and synoptic-scale short-lived events (e.g., atmospheric river events, atmospheric rivers) (Turner et al., 2019; Wille et al., 2021) and evident in the ice core records from coastal regions (Servettaz et al., 2020; Jackson et al., 2023). Moreover, the intensity and frequency of cyclone events also affect snowfall in Antarctic coastal areas (Dalaiden et al., 2020a). Particularly, in the Ross Sea region, the cyclonically driven SA is dominant and the region is sensitive to tropical and local climate drivers (Bertler et al., 2018). The contribution of synoptic-scale transport has been reported to be large for Victoria Land based on simulations over the 1985–2014 period (Dalaiden et al., 2020a). The influence of the ENSO on SA was evident at the Law Dome site (Roberts et al., 2015).

Based on the correlation of $\delta^{18}O$ in the GV7-C ice core with Nino 3.4, SOI, SAM, and SIE over the Ross-Amundsen Sea sector for 1957–2013 CE, the increasing (decreasing) $\delta^{18}O$ can be partly explained by the intrusion of relatively warm (colder) and moist (dry) air mass mainly through the PO sector of the Southern Ocean. This finding is comparable to other ice cores from the coastal Antarctica. In the Mount Brown South ice core in East Antarctica, evidence for moisture transport from the southern IO has been detectable from $\delta^{18}O$ signal, and the extreme precipitation events are linked with high-pressure systems in the mid-latitudes which increase the transport of warm and moist air mass from the southern IO (Jackson et al., 2023). In another

Line 349-350: A correlation is reported over the period 2005-2014 CE. Is this correlation (R=-0.24) statistically significant? If not, please remove it from the manuscript and report that “no statistically significant correlations were found” in that core over that period of time.

Line 351-353: Please add a reference to that line.

Answer: Thank you for the very helpful comments. We double checked and excluded it.

3.4 Discussion and implications

The variations in SA data from the GV7-C ice core showed significant interannual variations, and show only a weak correlation with IOD and SST-SEIO. The SA of the GV7-C ice core is assumed to be affected by the coupled influence of dynamic processes (i.e., the transport pathways and transport efficiency of moist air) or abrupt synoptic events (e.g., intense transport by atmospheric river events) (Turner et al., 2019; Wille et al., 2021). The variability in SA is affected by moisture transport via large-scale atmospheric circulation (Thomas et al., 2008; Udy et al., 2021; Cohen et al., 2012) and synoptic-scale short-lived events (e.g., atmospheric river events, atmospheric rivers) (Turner et al., 2019; Wille et al., 2021) and evident in the ice core records from coastal regions (Servettaz et al., 2020; Jackson et al., 2023). Moreover, the intensity and frequency of cyclone events also affect snowfall in Antarctic coastal areas (Dalaiden et al., 2020a). Particularly, in the Ross Sea region, the cyclonically driven SA is dominant and the region is sensitive to tropical and local climate drivers (Bertler et al., 2018). The contribution of synoptic-scale transport has been reported to be large for Victoria Land based on simulations over the 1985–2014 period (Dalaiden et al., 2020a). The influence of the ENSO on SA was evident at the Law Dome site (Roberts et al., 2015).

Based on the correlation of $\delta^{18}O$ in the GV7-C ice core with Nino 3.4, SOI, SAM, and SIE over the Ross-Amundsen Sea sector for 1957–2013 CE, the increasing (decreasing) $\delta^{18}O$ can be partly explained by the intrusion of relatively warm (colder) and moist (dry) air mass mainly through the PO sector of the Southern Ocean. This finding is comparable to other ice cores from the coastal Antarctica. In the Mount Brown South ice core in East Antarctica, evidence for moisture transport from the southern IO has been detectable from $\delta^{18}O$ signal, and the extreme precipitation events are linked with high-pressure systems in the mid-latitudes which increase the transport of warm and moist air mass from the southern IO (Jackson et al., 2023). In another ice core from Adélie Land covering the 1946–2006 CE period, decadal variations in $\delta^{18}O$ and regional temperature were correlated (Goursaud et al., 2017). Moreover, $\delta^{18}O$ shows a tendency to decrease with increasing wind speed. However, the $\delta^{18}O$ on an annual scale could not be explained by changes in the SIE and temperature, indicating the importance of site-dependent climate signals in coastal ice cores (Goursaud et al., 2017). In another study, isotope-based results indicated colder SSTs, a higher SIE, stronger katabatic winds, and decreasing SA in the Victoria Low Glacier ice core during the 1288–1807 period (the Little Ice Age period) (Bertler et al., 2011). Little Ice Age-related cooling is also evident in the $\delta^{18}O$ signal from the Hercules Neve ice core for the 1770–1890 period (Stenni et al., 1999) and frequent cold intervals in the Talos Dome ice core (Stenni et al., 2002). In line with these observations, a slight decreasing trend was observed in the $\delta^{18}O$ signal from the GV7-C ice core during the 1782–1845 CE period (Fig. 4), which may be part of Little Ice Age cooling. After 1845, there was no long-term trend in $\delta^{18}O$ from the GV7-C ice core; rather, values lower than the long-term mean were frequently observed (the blue lines in Fig. 4). This depletion of $\delta^{18}O$ observed from the GV7-C ice core may be possibly linked with changes in atmospheric circulation (e.g., SAM-related cooling) (Thompson and Solomon, 2002). Moreover, in terms of temperature reconstruction, $\delta^{18}O$ signal in the GV7-C ice core contrasts to anthropogenic global warming, suggesting more local/regional variations or various climatic factors.

Line 369: Please correct “is contrast” for “contrasts”

Answer: Thank you for the comment, we have edited accordingly.

core (Stenni et al., 2002). In line with these observations, a slight decreasing trend was observed in the $\delta^{18}O$ signal from the GV7-C ice core during the 1782–1845 CE period (Fig. 4), which may be part of Little Ice Age cooling. After 1845, there was no long-term trend in $\delta^{18}O$ from the GV7-C ice core; rather, values lower than the long-term mean were frequently observed (the blue lines in Fig. 4). This depletion of $\delta^{18}O$ observed from the GV7-C ice core may be possibly linked with changes in atmospheric circulation (e.g., SAM-related cooling) (Thompson and Solomon, 2002). Moreover, in terms of temperature reconstruction, $\delta^{18}O$ signal in the GV7-C ice core contrasts to anthropogenic global warming, suggesting more local/regional variations or various climatic factors.

Lines 372-373: The sentence in these lines reports Southern Ocean warming co-varying with dexcess during 1991-2000 CE. While this statement may support the authors point, it also raises questions about the co-variability of these parameters outside those 10 years. Please, add more information about the Southern Ocean warming vs d-excess relationship outside that 10 year window.

Answer: Thank you for the comment, we meant here to elaborate the relationship (positive) between d-excess and SST. We then excluded the 1991-2000 CE period.

Based on the correlation of *d*-excess with SST-SEIO and SST anomaly (Tables 4 and 6), the *d*-excess signal from the GV7-C ice core likely to preserve the thermodynamic changes (i.e., SST changes) particularly over the IO sector of the Southern Ocean. Notably, the southern Indian Ocean exhibits the most intense cyclonic activity in the Southern Ocean, which may enhance the detectability of this signal in the *d*-excess record (Simmonds et al., 2003). *D*-excess as an indicator of climate conditions in the source region (Jouzel et al., 1982; Sodemann and Stohl, 2009; Lewis et al., 2013), warming over the Southern Ocean, was found to co-vary with higher *d*-excess in the Victoria Lower Glacier ice core (Bertler et al., 2011). At the Law Dome ice core site, *d*-excess also reflects SST changes over the southern IO sector (Masson-Delmotte et al., 2003). Particularly the abrupt increase in the *d*-excess in the 1970s was consistent with the *d*-excess of the GV7-C ice core. This relevance was explained by the abrupt changes in meridional atmospheric circulation, which led to the intrusion of warm subtropical moisture sources to the Antarctic coast during the 1970s (Masson-Delmotte et al., 2003). Consistently large peaks in the five-year

Line 375: The line states "… was consistent with the GV7-C ice core result". Please specify to which result you are referring to.

Answer: Thank you for the comment, we have edited accordingly.

Based on the correlation of *d*-excess with SST-SEIO and SST anomaly (Tables 4 and 6), the *d*-excess signal from the GV7-C ice core likely to preserve the thermodynamic changes (i.e., SST changes) particularly over the IO sector of the Southern Ocean. Notably, the southern Indian Ocean exhibits the most intense cyclonic activity in the Southern Ocean, which may enhance the detectability of this signal in the *d*-excess record (Simmonds et al., 2003). *D*-excess as an indicator of climate conditions in the source region (Jouzel et al., 1982; Sodemann and Stohl, 2009; Lewis et al., 2013), warming over the Southern Ocean, was found to co-vary with higher *d*-excess in the Victoria Lower Glacier ice core (Bertler et al., 2011). At the Law Dome ice core site, *d*-excess also reflects SST changes over the southern IO sector (Masson-Delmotte et al., 2003). Particularly the abrupt increase in the *d*-excess in the 1970s was consistent with the *d*-excess of the GV7-C ice core. This relevance was explained by the abrupt changes in meridional atmospheric circulation, which led to the intrusion of warm subtropical moisture sources to the Antarctic coast during the 1970s (Masson-Delmotte et al., 2003). Consistently large peaks in the five-year

Lines 389-390: Please check this sentence for clarity

Answer: Thank you for the comment, we have edited accordingly.

Based on various correlation analysis with the climate variables used in this study, the following interpretations are summarized. During the period 1957–2013 CE, the correlation patterns based on SA, $\delta^{18}O$, and *d*-excess support that snow precipitating at the GV7-C site mainly originates from the Southern Ocean possibly via western PO and southeastern Indian Ocean. For the longer time scale (1872–2013), the correlation patterns based on *d*-excess for SST indicates more detectability of air mass intrusion from the Indian Ocean sector of the Southern Ocean. This suggests a warmer (colder) ocean surface condition would be preserved in higher (lower) $\delta^{18}O$ (recent period) and *d*-excess values (recent and longer period) in the GV7-C ice core.

Lines 396-397: Please add a reference to this line.

Answer: Thank you for the comment, we have added.

3.4 Discussion and implications

The variations in SA data from the GV7-C ice core showed significant interannual variations, and show only a weak correlation with IOD and SST-SEIO. The SA of the GV7-C ice core is assumed to be affected by the coupled influence of dynamic processes (i.e., the transport pathways and transport efficiency of moist air) or abrupt synoptic events (e.g., intense transport by atmospheric river events) (Turner et al., 2019; Wille et al., 2021). The variability in SA is affected by moisture transport via large-scale atmospheric circulation (Thomas et al., 2008; Udy et al., 2021; Cohen et al., 2012) and synoptic-scale short-lived events (e.g., atmospheric river events, atmospheric rivers) (Turner et al., 2019; Wille et al., 2021) and evident in the ice core records from coastal regions (Servettaz et al., 2020; Jackson et al., 2023). Moreover, the intensity and frequency of cyclone events also affect snowfall in Antarctic coastal areas (Dalaiden et al., 2020a). Particularly, in the Ross Sea region, the cyclonically driven SA is dominant and the region is sensitive to tropical and local climate drivers (Bertler et al., 2018). The contribution of synoptic-scale transport has been reported to be large for Victoria Land based on simulations over the 1985–2014 period (Dalaiden et al., 2020a). The influence of the ENSO on SA was evident at the Law Dome site (Roberts et al., 2015).

Line 411: The line states “It is useful…”. Please specify “what is useful” or reassess the sentence for clarity.
Citation: https://doi.org/10.5194/egusphere-2025-2408-RC2

Answer: Thank you for the comment, we have edited this paragraph which quite wordy and ambiguous.

Lastly, it is notable that the importance of the GV7-C ice core records in climate studies. The historical temperature variability over the tropical ocean is important for global warming scenarios (IPCC, 2019). The projections show oceanic and atmospheric warming (Timmermann and Hellmer, 2013), and heat transported by the Southern Ocean further induces the melting of Antarctic ice shelves (Rignot et al., 2019). Particularly, the IO is experiencing the strongest and most robust warming (Du and Xie, 2008; Beal et al., 2019), largely driven by anthropogenic forcing (Dong et al., 2014), and it is projected to warm non-uniformly (Sharma et al., 2023). The IO and the PO temperature anomaly affects the surface air temperature of Antarctica (Zhang and Duan, 2023). Moreover, warm SSTs in the western tropical IO excite a poleward-moving Rossby wave, inducing the changes in sea ice extent (Zhang et al., 2024). The coastal and inland Antarctic regions emerge an anomalous retreat of sea ice extent and warming due to the short-term significant intrusion of warm and moist air masses associated with strong negative phase of SAM (Ionita et al., 2018). The SAM variation in the recent period is unprecedented in the last millennia (Fogt and Marshall, 2020) and the increasing influence of the SAM-ENSO coupling has been reported since the 1940s (in coastal Dronning Maud Land) (Ejaz et al., 2022). Thus, understanding the response of the Antarctic climate to ocean variability of the IO sector would be important.

We appreciate all comments and suggestions on our manuscript. We are looking forward to its publication. Thank you for handling our manuscript and your patience.

Sincerely,
Jeonghoon Lee